Solid Earth, 15, 1385–1406, 2024
https://doi.org/10.5194/se-15-1385-2024

Solid Earth Open Access EGU

Geophysical downhole logging analysis within the shallow-depth ICDP STAR drilling project (central Italy)

Paola Montone[1], Simona Pierdominici[2], M. Teresa Mariucci[1], Francesco Mirabella[3], Marco Urbani[3], Assel Akimbekova[3], Lauro Chiaraluce[1], Wade Johnson[4], and Massimiliano Rinaldo Barchi[3]

[1]Istituto Nazionale di Geofisica e Vulcanologia, 00143 Rome, Italy
[2]GFZ, German Research Centre for Geosciences, Telegrafenberg, 14473 Potsdam, Germany
[3]Dipartimento di Fisica e Geologia, Università degli Studi di Perugia, 06123 Perugia, Italy (member of CRUST – Centro inteRUniversitario per l'analisi SismoTettonica tridimensionale con applicazioni territoriali)
[4]EarthScope Consortium, Boulder, CO 80301, USA

Correspondence: Paola Montone (paola.montone@ingv.it)

Received: 26 April 2024 – Discussion started: 13 May 2024
Revised: 10 September 2024 – Accepted: 30 September 2024 – Published: 27 November 2024

Abstract. The International Continental Scientific Drilling Program (ICDP) STAR (A Strainmeter Array Along the Alto Tiberina Fault System) drilling project aims to study the seismic and aseismic fault slip behavior of the active low-angle Alto Tiberina normal fault (ATF) in the northern Apennines, central Italy, by drilling and instrumenting six shallow boreholes (maximum depth 160 m) with seismometers and strainmeters. During the STAR fieldwork, a geophysical downhole logging campaign was carried out to define the optimal target depth for instrument deployment and formation rock characterization. In particular, the main objectives of this study were to define in situ physical properties of the rocks and the tectonic discontinuity geometry along the boreholes. The downhole logging data provide new findings and knowledge, especially with regards to physical properties such as resistivity and gamma-ray and wave velocity. The collected parameters were compared to the results of literature data collected in similar lithologies, as well as with the results of logging performed in deeper wells drilled for commercial purposes. The physical properties of the Mesozoic–early Tertiary calcareous formations show low gamma-ray values and high compressional (Vp) and shear wave (Vs) velocities (up to 5.3 and 2.9 $\mathrm{km\,s^{-1}}$, respectively), whereas the overlying clay-rich Late Tertiary formations exhibit high gamma-ray and low resistivity values as well as relatively low Vp and Vs values (up to 3.5 and 2.0 $\mathrm{km\,s^{-1}}$, respectively). The results obtained from the analysis of the orientations of the tectonic structures, measured along the six boreholes, show good agreement with the orientations of the present-day extensional stress field, which is NE–SW-oriented. Our study allowed us to bridge the gap between the physical properties obtained from literature data and those obtained from the deep well measurements, representing a possible case history for future projects. These new outcomes represent an almost unexplored window of data and will contribute to the advancement of knowledge of the physical properties of the rocks at shallow depths, which are typically overlooked.

1 Introduction

The aim of the STAR drilling project (A Strainmeter Array Along the Alto Tiberina Fault System) is to study seismic and aseismic slip on active high- and low-angle seismogenic normal faults (Chiaraluce et al., 2024) in central Italy, an area affected by seismic events with magnitude up to M_w 6.6 (Fig. 1). The STAR drilling project is an international effort contributing to the infrastructural implementation of the Alto Tiberina Near Fault Observatory (TABOO-NFO) (Chiaraluce et al., 2014a, b, 2022), a long-term research infrastructure mapped by the EPOS (European Plate Observing System) initiative as one of the European Solid Earth Science facilities providing open-access data to the international community (http://www.epos-eu.org, last access: 22 November 2024). STAR is one of the International Continental Scientific Drilling Program (ICDP) projects with a pri-

mary focus on long-term borehole monitoring of fault-zone deformation (e.g., Bohnhoff et al., 2017; Fischer et al., 2022).

To improve comprehension of the processes controlling fault mechanics and earthquake generation, the STAR drilling project installed short-period (2 Hz) seismometers (three-component borehole geophones) and strainmeters (Gladwin Tensor Strainmeters, GTSMs) in six shallow boreholes (maximum depth 160 m) that were purpose-drilled. The seismometers were installed to monitor and record the seismicity of the low-angle Alto Tiberina normal fault (ATF) and its main antithetic splay, the Gubbio normal fault (Mirabella et al., 2004; Caricchi et al., 2015) (Fig. 2). Borehole strainmeters were deployed because they are the only instruments able to measure small creep events, as demonstrated in similar experiments focused on other faults, such as the creeping section of the strike-slip San Andreas Fault near Parkfield (Langbein et al., 2006). Small creep events can be recorded by strainmeters, whose high resolution, for periods of hours to ~ 10 d, enables the identification of subtle, time-varying crustal deformations that are too small to be measured by GNSS or InSAR. Seismic and strain observations from STAR borehole monitoring will be integrated with regional observations on active seismicity, on deep crustal structure, and on the present-day stress field.

The locations of the six boreholes were selected based on two main criteria: on a regional scale, the objective was to enhance understanding of the seismic behavior of the ATF; on a local scale, the primary requirement was to deploy the instruments while avoiding areas of inhomogeneous, anisotropic, or highly fractured rock volumes (Chiaraluce et al., 2024). The six 80–160 m shallow monitoring boreholes, named TSM01–TSM06, (see locations in Fig. 1) were drilled surrounding the creeping portion of the ATF in two phases: during the fall of 2021 and spring of 2022. The STAR drilling operations were supported by the acquisition in all the boreholes of a wide set of geophysical logs including an optical borehole imager (OBI), acoustic borehole imager (ABI), caliper (CAL), gamma-ray (GR), fluid temperature–conductivity (FTC), sonic (FWS), resistivity, and spontaneous potential (ELOG) logs. The borehole geophysical measurement purposes for the STAR drilling project were twofold: firstly, to characterize the physical properties of the rock formation in the subsurface and, secondly, to identify an intact and competent fracture-free interval in each borehole in which to deploy the strainmeter and seismometer. After the completion, each borehole was instrumented and ready for data acquisition (Chiaraluce et al., 2024).

The objective of this paper is to provide a critical overview of the physical properties of the in situ rock formations and their fracture characteristics based on analysis and interpretation of downhole logging data. Particular attention was paid to optical and acoustic image logs with the aim of identifying intact rock and structural discontinuities. In fractured rock masses, discontinuities have significant control over the rock mass behavior. Mapping the fractures and their geometry at depth helped us identify optimal intervals to host seismometers and strainmeters. In order to work properly and obtain reliable data, these instruments must have a perfect coupling with the rock mass: therefore, borehole seismic installations have to take into account the borehole diameter and tilt, temperature profile, lithology, and fracture distribution.

In this paper, after a brief description of the seismicity of central Italy and a geological and tectonic overview of the area where the boreholes are located, we describe the main results of the operated logging. Geophysical downhole measurements provide a contribution to better define the physical properties of the Umbria–Marche carbonate multilayer (mainly limestones and marls) and of the overlying turbidites, cropping out in this area. These results are then compared with the analog measurements, acquired in much deeper boreholes, drilled in the same region for hydrocarbon exploration purposes, as well as with the available recently acquired laboratory measurements (e.g., De Paola et al., 2009; Smeraglia et al., 2014; Trippetta et al., 2010, 2021) relating to the effects of the confining pressure on the physical parameters of the rocks. In particular, the results related to the P-wave velocities obtained from the sonic log readings along the six STAR boreholes have been compared with the previous results related to the same geological formations (e.g., Barchi et al., 1998; Diaferia et al., 2006; Bigi et al., 2011; Mirabella et al., 2011; Scisciani et al., 2014; Porreca et al., 2018; Montone and Mariucci, 2020; Trippetta et al., 2021). From the geophysical log analysis, we have defined and characterized several planar discontinuities along each borehole, related to either primary (bedding) or secondary (tectonic) structures (fault and/or fractures). The orientations of the tectonic structures, recognized along the boreholes, have been considered together with other available data and compared with the present-day stress field.

Summarizing, our paper aims to bridge the gap between the physical properties obtained from literature data (e.g., laboratory analyses) for outcrop samples and those obtained from the wellbore measurements of oil and gas companies (such as AGIP and ENI; https://www.videpi.com/videpi/pozzi/consultabili.asp, last access: 20 August 2024), which investigate significantly greater depths. The new data in this study will contribute to the advancement of knowledge of the physical properties of the rock volumes at relatively shallow depths (0–200 m), which are typically overlooked. Beyond the specific case reported here, geophysical and petrophysical data acquired in shallow boreholes also contribute to the knowledge of the upper crust. Indeed, they provide in situ measurements linking data obtained for outcropping rocks, often influenced by surface processes, to those from deep wells. Our study shows how even with relatively few data in a large area, valuable insights can be obtained. With more data in a region of interest, we would be able to shed light on a complete portion of the crust, from the surface to a few kilometers of depth or even deeper. Overall, also considering the results obtained in the analysis and interpreta-

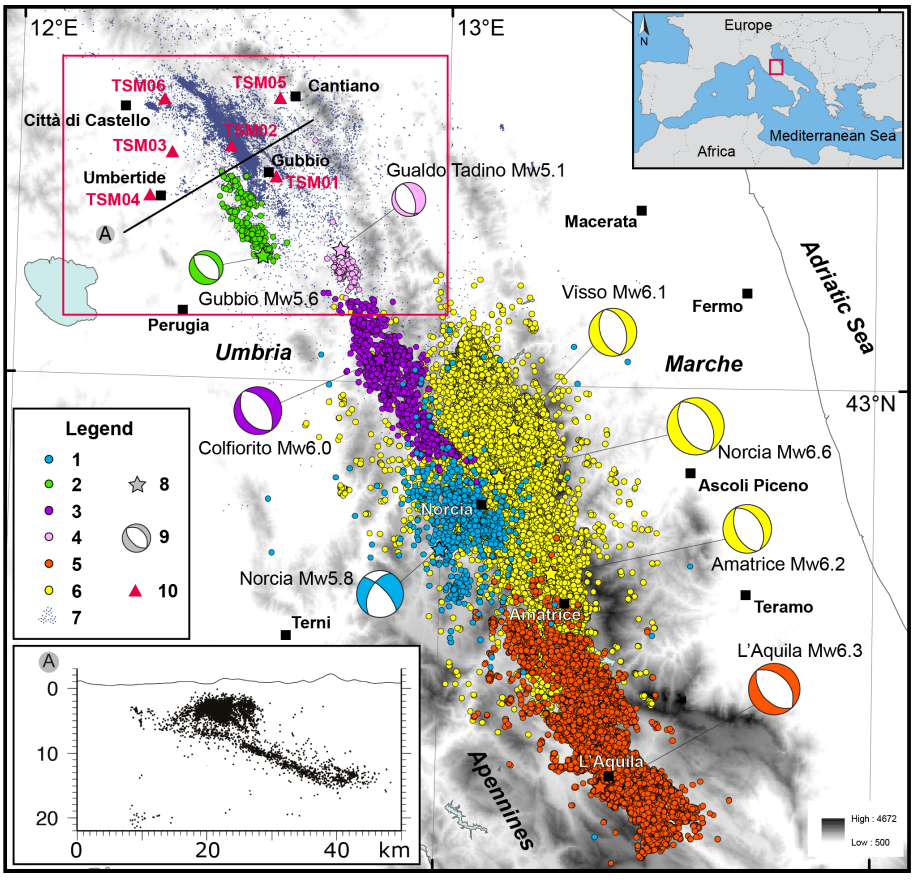

Figure 1. Seismicity in the study area and main seismic sequences in central Italy in the last 45 years. Legend (1 to 6 are earthquakes): 1 – Norcia 1979 (Deschamps et al., 1984); 2 – Gubbio 1984 (Haessler et al., 1988); 3 – Colfiorito 1997 (Chiaraluce et al., 2003); 4 – Gualdo Tadino 1998 (Ciaccio et al., 2005); 5 – L'Aquila 2009 (Valoroso et al., 2013); 6 – central Italy 2016–2017 (Michele et al., 2020); 7 – seismicity in the period 2010–2014 (Valoroso et al., 2017); 8 and 9 – location of main events of the sequences and related focal mechanisms (http://www.bo.ingv.it/RCMT/Italydataset.html, last access: 1 April 2024; Pondrelli and Salimbeni, 2006; Pondrelli et al., 2006; http://autorcmt.bo.ingv.it/quicks.html, last access: 1 April 2024); 10 – STAR boreholes (TSM). The red box is the area of Fig. 2. In the lower left corner is a cross-section of the seismicity (Michele et al., 2020).

tion of the data in this study, the outcomes from the STAR drilling project will provide a better understanding of the behavior of the main active faults, addressing fundamental questions about the relationship between creep, slow slip, dynamic earthquake rupture, and tectonic faulting (Anderlini et al., 2016; Chiaraluce et al., 2024).

2 Seismotectonic and geological framework of the area

Seismicity in central Italy is mainly characterized by shallow crustal earthquakes (5–15 km depth) localized along the Apennine belt with maximum magnitudes of about 6.6 (Chiarabba et al., 2005; Chiaraluce et al., 2017b). Earthquake focal mechanisms show a prevalent normal-faulting regime, with a NE–SW-striking extension, consistent with other data characterizing the active stress field in this area, such as breakouts and active faults (Mariucci and Montone, 2024).

In the last 45 years, central Italy has experienced several crustal normal-faulting earthquakes (Fig. 1), causing surface faulting as well as visible fractures and significant damage (Cinti et al., 1999; Barchi and Mirabella, 2009; Boncio et al., 2010; Emergeo working Group, 2010; Pizzi et al., 2017; Villani et al., 2018; Barchi and Collettini, 2019). The most significant earthquakes that occurred in the past, with a moment magnitude greater than 5.5 (Fig. 1), are the M_w 5.8 Norcia in 1979, the M_w 5.6 Gubbio in 1984, and the seismic sequence of Colfiorito–Gualdo Tadino in 1997–1998, with the largest event being M_w 6.0 (Cello et al., 1997; Amato et al., 1998; Amato and Cocco, 2000; Boncio and Lavecchia, 2000; Ciaccio et al., 2005; Mildon et al., 2016). Finally, the seismic sequence that began in 2016 in Amatrice (Tinti et al., 2016; Chiaraluce et al., 2017a; Chiarabba et al., 2018) occurred with three main events (M_w 6.2 in Amatrice, M_w 6.1 in Visso, and M_w 6.6 in Norcia), causing about 300

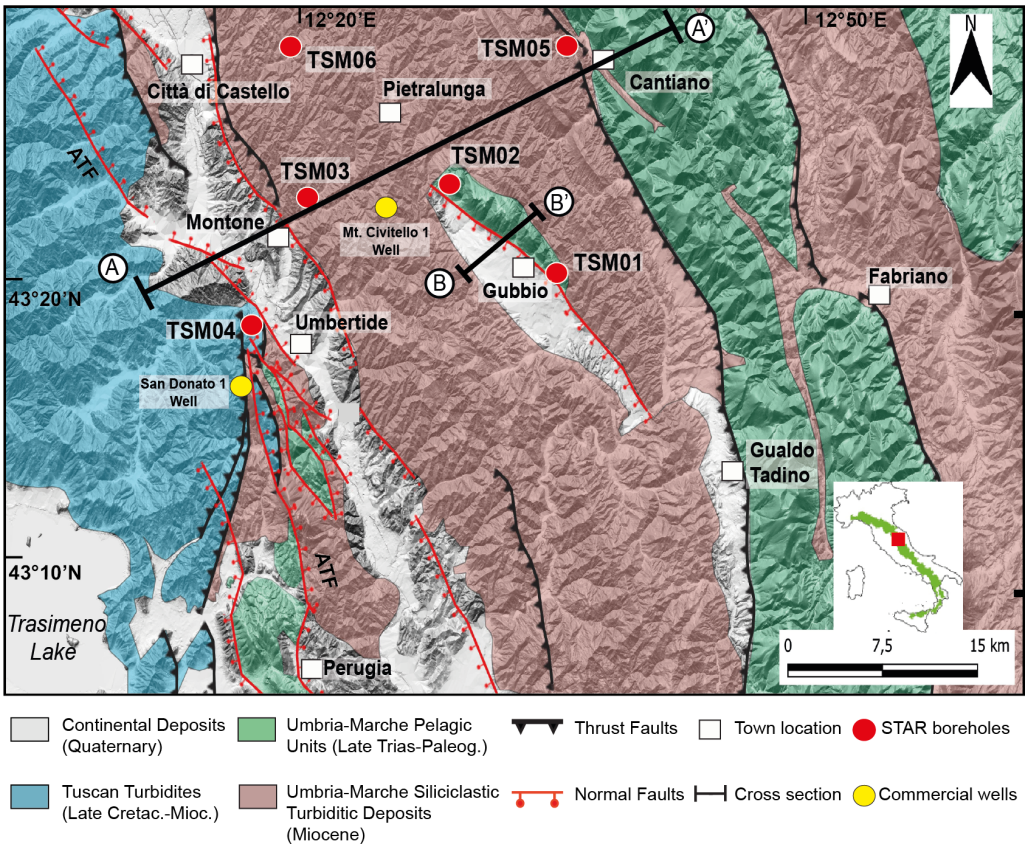

Figure 2. Geological setting of the study area. The locations of the six STAR boreholes (red circles) drilled in fall 2021 (TSM01, TSM02, and TSM03) and in summer 2022 (TSM04, TSM05, and TSM06), as well as the two deep commercial boreholes (yellow circles) San Donato 1 and Mt. Civitello 1, are displayed. Modified from Mirabella et al. (2011). ATF is the Alto Tiberina fault. The geological cross-sections A-A′ and B-B′ are in Fig. 3.

deaths, injuries, and the destruction of numerous historic centers (Fig. 1).

The six boreholes of the STAR drilling project were drilled in the NW part of the actively extending area of the Umbria–Marche Apennines (Fig. 2), a NE-verging, arc-shaped foreland fold-and-thrust belt representing the eastern part of the northern Apennines of Italy. Within the study area the compressional structures (folds and thrusts) are mostly arc-shaped with a roughly NNW–SSE trend and were formed in Late Miocene (Tortonian–Messinian age). They affect a pre-orogenic Jurassic–Paleogene carbonate multilayer (Umbria–Marche succession) (e.g., Cresta et al., 1989), overlain by a thick succession of synorogenic Neogene turbidites, marls, and sandstones deposited in the northern Apennines foreland basin (e.g., Barchi, 2010). The compressional structures are cut and displaced by later (Late Pliocene–Quaternary) NW–SE-striking normal faults, which are related to an extensional stress field oriented in a NE direction, responsible for the present-day seismicity of the region. The normal fault attitude is consistent with the extensional stress regime inferred from earthquake focal mechanisms and borehole breakouts (Mariucci et al., 2008; Montone and Mariucci, 2016; Villani et al., 2018).

The most prominent normal fault exposed in the study area is the SW-dipping Gubbio fault, down-throwing the western backlimb of the Gubbio anticline (Fig. 3). The Gubbio fault is antithetic to a major NE-dipping extensional detachment, i.e., the ATF (e.g., Mirabella et al., 2011; Lavecchia et al., 2017; Vuan et al., 2020). The fault dip of less than 30° makes the ATF an unfavorably oriented geological structure for reactivation with respect to the regional stress field. The ATF and its high-angle antithetic splays release continuous microseismicity and rarer moderate sequences, e.g., in 1984 (Haessler et al., 1988) and in 2010–2014 (Marzorati et al., 2014).

The stratigraphy of the study area, from top to bottom, can be summarized as follows (Barchi, 2010): (i) marine and continental Plio-Quaternary sediments, mainly clays and sands in different combinations and with different degrees of compaction; (ii) a thick Neogene synorogenic turbidite succession, namely the Marnoso–Arenacea Fm. (Miocene), formed of alternated shales and sandstones, with strong vertical and lateral variability; (iii) a hemipelagic marly succes-

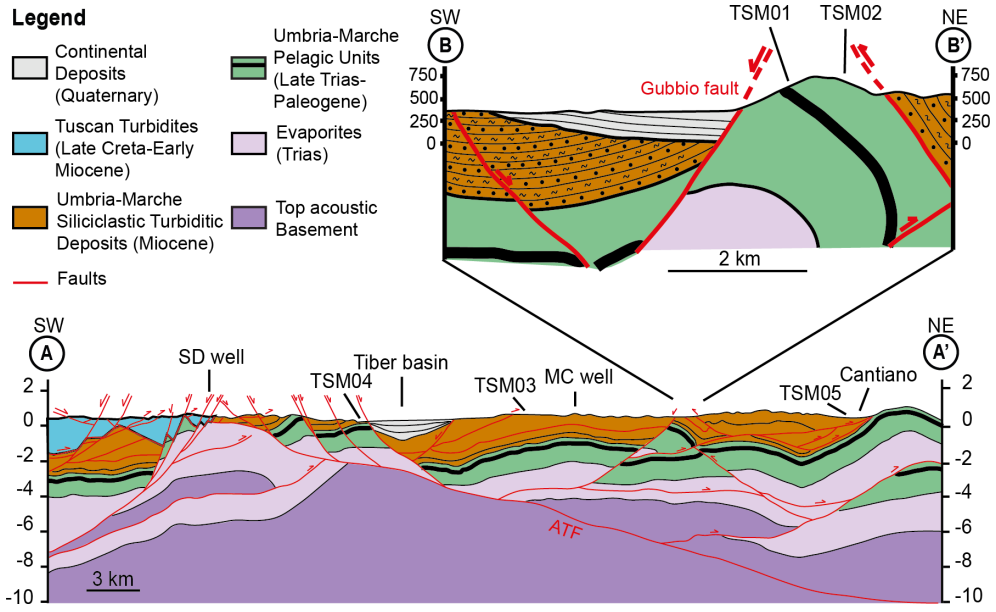

Figure 3. Geological cross-sections (A-A′ and B-B′ in Fig. 2). The geometry at depth of the main tectonic structures such as the Alto Tiberina low-angle normal fault (ATF) and the Gubbio fault (Mirabella et al., 2011) is shown. SD well: San Donato 1 well; MC well: Mt. Civitello 1 well.

sion (Schlier, Bisciaro, and Scaglia Cinerea Fms.; Eocene–Miocene); (iv) a carbonate pelagic sedimentary sequence of the Umbria–Marche domain (Mesozoic–Paleogene) that includes not only limestone and chert-bearing limestone but also marl and clay (Scaglia Variegata, Scaglia Rossa, Scaglia Bianca, Marne a Fucoidi, and Maiolica Fms.); (v) Lower Jurassic massive platform carbonate (Calcare Massiccio Fm.); (vi) an Upper Triassic evaporitic succession, consisting of alternated anhydrites and dolostones (Anidriti di Burano Fm.); and (vii) Middle Triassic and/or older continental and shallow marine meta-sediments (Verrucano Fm. sensu lato).

Within the STAR study area (Figs. 2 and 3), two deep wells (San Donato 1 and Mt. Civitello 1) were drilled in the past by Italian oil companies. The well stratigraphy is schematically reported in previous literature (e.g., Mariucci et al., 2008; Mirabella et al., 2011; Caricchi et al., 2015). The San Donato 1 well (SD), reaching a depth of 4763 m, was drilled by SNIA–BPD in 1983–1984 and is located approximately 20 km southwest of the Mt. Civitello 1 well (MC). The SD well is situated very close to the ATF, intersecting it at a depth of 326 m, where the Miocene Marnoso–Arenacea turbidites directly overlie the Triassic evaporitic succession, extending down to a depth of about 3000 m. At greater depth, the well penetrates the metamorphic acoustic basement in tectonic contact with the evaporitic succession (Fig. 3). The MC well, drilled by AGIP in 1988–1989, located near the Gubbio fault, reaches a depth of 5600 m. From the surface to a depth of about 1000 m, the well crosses the turbidite succession. Then the well passes through the carbonate Meso-Cenozoic pelagic sequence. From about 2800 m to the bottom at 5600 m, the well crosses the Triassic evaporitic succession.

3 Method: downhole logging processing and analysis

Knowledge of the petrophysical properties of the different lithostratigraphic units is an important aspect to understand the subsurface. In the absence of coring material, as in the STAR project, data acquisition from downhole logging becomes the key element in determining the rocks' physical characterization (Rider and Kennedy, 2011). Downhole logging is a method to gain continuous, in situ, high-resolution data on various physical or structural rock parameters collected within a borehole. For the STAR drilling project, the downhole logging was performed for all six boreholes in order to allow detailed sedimentary facies assessment and to identify the best location to deploy the strainmeters and seismometers at depth. All six boreholes were logged by slim-hole sondes (for details see Table S1 and text in the Supplement) and following the standard methods in this field (Serra, 1984; Ellis and Singer, 2007; Rider and Kennedy, 2011; Schön, 2015; Pierdominici and Kück, 2021). Downhole measurements were conducted in each borehole after the drilling operations and executed mainly in the open-hole (OH) sections; only GR also ran in the cased section (CH). The following downhole measurements were successfully recorded: total gamma-ray (GR) values, full-waveform sonic profile (Vp and Vs), temperature (T) and conductivity (COND), three-arm caliper (CAL), resistivity (RESIST), single-point resistance (SPR), and acoustic (ABI) and optical

images (OBI). We have summarized the logging measurements and logged interval for each borehole in Table S1. For the drilling operations, water was used as a drilling fluid, allowing the OBI to run. Borehole quality has been determined by vertical and horizontal deviation of the borehole and the condition of the borehole wall. In order to pursue the objective of the STAR drilling project and for proper use and performance of the instruments, all six boreholes were drilled within 5° from the vertical. The deviation of each borehole was then checked as part of the logging program. The boreholes have an inclination of less than 2° except for the borehole TSM06 where the inclination is between 4.3 and 5.1°. Based on (i) the smooth borehole wall, (ii) logs without intervals of large washouts, and (iii) internal consistency for several tools (i.e., three different types of borehole diameter measurement), we infer that the log quality and reliability are very good for almost all sondes over the entire length of each hole.

Below, we summarize the main scientific purpose of each sonde.

The total gamma-ray (GR) log measures the natural radioactivity of the rock. The GR comes from the radioactive isotopes of potassium (^{40}K), uranium (^{238}U decay series), and thorium (^{232}Th decay series). Potassium is found primarily in clay minerals, micas, and potassium feldspar. Thorium is commonly associated with clay minerals and volcanic ash layers. Uranium is found in heavy minerals, glauconite, and organic-rich intervals and may be bound to clay. Relatively high values in the GR log are often associated with the influx of clay and coarser materials, while relatively low GR values generally indicate sedimentation of biogenic carbonate, organic carbon, or silica (e.g., Rider and Kennedy, 2011). We performed the GR log to detect layers of clay and to identify changes in lithology. GR was also recorded in drill pipes of all six STAR boreholes, although the signal appears a bit dampened. In essence, a GR log characterizes the different lithology crossed by the borehole, allowing for the identification of layers (thickness and lithotype) through the different clay content.

A three-arm caliper (CAL) sonde was used to measure the borehole diameter and to determine how smooth the borehole walls are. The strainmeter requires relatively smooth walls with no blowouts or fractures.

The fluid temperature–conductivity (FTC) measures the temporary temperature and conductivity of the borehole fluid. Both parameters can show strong variations caused by drilling activities inside the hole but can also detect the flow of fluids into or out of the formation. These logs are good indicators of areas of active flow or open fractures; they are therefore used to exclude areas or intervals with major fractures that would have affected both instrument placement and data quality.

The ELOG sonde – including RES and SPR – measures the rock capability to conduct electric currents. The tool provides resistivity profiles with four different depths of investigation. This measurement provides information about permeability, porosity, water types, and geological formation properties. In particular, in massive rocks with very low matrix porosity and permeability, the resistivity logs identify fluid-filled fracture zones (fracture permeability). So, we ran this logging sonde for the same reason as the FTC. Only for the TSM01 and TSM02 boreholes were no ELOG logs acquired.

The full-waveform sonic (FWS) sonde measures the velocity of sound waves through the rocks, which varies depending on lithology, rock texture, and porosity. The sonic velocity measurement is used for identification of compaction of lithologies, facies recognition, and fracture identification. The velocity has been determined by measuring the travel time of sonic pulses between transmitters and four receivers. We have reprocessed the raw sonic waveforms to estimate the P- and S-wave velocities using a combination of first arrival trace picking for P and S waves, along with additional semblance analysis.

Borehole image sondes provide a continuous oriented high-resolution image of the borehole walls (see the figures related to the boreholes, e.g., Fig. 6). Images collected in the STAR project have been obtained from acoustic (ABI) and optical (OBI) tools. The latter acquires a true-color optical image of the borehole wall, and the acquired data are displayed in one oriented unwrapped image. The sonde operates only in a transparent drilling fluid like fresh water or air. For TSM04 and TSM06 boreholes no optical image is available due to the high turbidity of the drilling water. The acoustic image data are visualized as two 360° north-oriented images (travel time and amplitude) of the borehole wall versus depth. The travel time (TT) provides information about the borehole shape, and the acoustic amplitude (AMPL) depends on the roughness and shape of the borehole wall and its acoustic properties, which depend on variations with texture, mineralogy, compaction, and fracturing (e.g., Davatzes and Hickman, 2010; Mcginnis et al., 2017; Medici et al., 2023). These AMPL and TT images are visualized in colors based on their value range. Here, in the AMPL image, strong contrast (high amplitude, bright color) indicates a strong signal and good reflection, and low contrast (low amplitude, dark color) indicates weak to missing signals (scattered or absorbed impulse). In the TT image, the bright colors indicate a short time period (fast) for the impulse to go from the transducer and back to the receiver; the dark colors represent a long time period (slow), which means a widened size of the borehole (e.g., Pierdominici et al., 2020). Each planar discontinuity, such as fracture, fault, or bedding, appears in the images as sine waves (e.g., Davatzes and Hickman, 2010). To obtain a correct geometry of the planar structures (dip azimuth and dip) the TT and AMPL images have been previously corrected by diameter, inclination, and orientation of the borehole. We have grouped the features into six categories (see Sect. 4.3): open (in red), filled (in gray), bedding (in green), stylolite (in turquoise), cherty layer (in dark gray),

and weak zones. The acoustic imager tool alone cannot distinguish between open or closed/filled structures (used here in a general sense, i.e., including faults, fractures, and veins). Based on the comparison of these two images, we might distinguish so-called "open" structures based on their contrast with ultrasonic AMPL and the corresponding response in the TT. The structures defined as "closed" are visible only in the amplitude image. To enhance the travel time and amplitude images, static and dynamic (10 cm vertical window) normalizations were applied. Raw, static, dynamic images display minor differences from each other in the resulting images depending on the scale and variations between different intervals and features. The displayed images here refer to the static normalization. ABI and OBI were also used to determine the borehole trajectory based on a borehole's deviation from vertical (DEVI) and the direction of this deviation with respect to magnetic north (hole or drift azimuth; HAZI). For the installation of strainmeters and seismometers, all STAR boreholes had to be very close to the vertical. Thus, this type of acquisition played a key role in knowing the condition of the borehole and determining the successful installation of the instruments.

4 Data and results

4.1 Borehole description

Six STAR boreholes were drilled surrounding the creeping portion of the ATF to deploy strainmeters and seismometers (Fig. 1) in order to improve our understanding of the ATF seismicity pattern and monitor the evolution of seismicity in this area over time (Chiaraluce et al., 2024). For the location of our six boreholes, we followed two criteria: at a regional scale, three boreholes (TSM01, TSM02, and TSM06) are located following the axis of the Gubbio anticline and its northern continuation, and the others (TSM03, TSM04, and TSM05) are where the maximum extension rate is expected. At a local scale, the instruments were deployed in relatively homogeneous lithology, avoiding complex formations (e.g., alternating stiff and weak rocks or limestones and marl layers) as well as anisotropic or highly fractured rock intervals. The downhole logging measurements were performed immediately after drilling and prior to instrument installation. A posteriori, the known mechanical properties of the rocks hosting the instruments will be used to improve the interpretation of the data recorded.

The boreholes are located within an area of about 1500 km^2, centered around the town of Gubbio (Fig. 2 and Table S2). TSM01 and TSM02, near the Gubbio fault, were drilled across the late Mesozoic–early Tertiary carbonates, cropping out along the crest of the Gubbio anticline (Fig. 4a and b). The other boreholes were drilled in the Tertiary marls and sandstones, cropping out in the northern part of the study area: TSM04 is located on the footwall of the ATF, TSM03 and TSM06 were drilled on the ATF hanging wall, and TSM05 is located in the farthest part of the ATF close to the western flank of the Umbria–Marche ridge (Fig. 4c–f; for more detail, see Chiaraluce et al., 2024). See the Supplement for a detailed lithological description (Sect. S1 in the Supplement).

4.2 Log results

The downhole logging data are described and interpreted to provide new findings and knowledge to complement those obtained from similar rock types sampled in the field outcrops (Figs. 5 and 6–9).

Results from the downhole logging analysis are summarized in Tables 1 and S1, displaying the average values and the related standard deviation. More details are described in Sect. S2 in the Supplement.

GR log response (open and cased hole) in TSM01 and TSM02 boreholes is generally very low (Fig. 5, Table 1). In TSM01, the low GR, associated with the limestone Scaglia Bianca Fm., slowly increases in the marly Marne a Fucoidi Fm., proportionally to the enrichment of the clay component as evidenced in the interval between 55.0 and 66.5 m. The sharp contact between the Marne a Fucoidi Fm. and the underlying limestone Maiolica Fm. is well indicated by the dramatic decrease in GR values (from 50 cps for the Marne a Fucoidi Fm. to 14 cps for the Maiolica Fm.). The open-hole section intersects only the Maiolica Fm., with an average GR value of 8.4 cps. In TSM02, GR records a very low response related to the three pelagic formations intersected, predominantly consisting of limestones, which are interbedded with sporadic, relatively thin marly layers as recorded by the increase in GR values (e.g., 73–75 m, 102–104 m, and 134–135 m for the Scaglia Rossa Fm.). In the TSM03, TSM04, TSM05, and TSM06 boreholes, the GR log shows higher values which vary between 49 cps in TSM05 and 104 cps (open hole) in TSM03. The GR values are lower in the cased section because the signal is damped by casing. In the open-hole section, on the other hand, the GR response for all four boreholes is generally high, displaying relatively uniform values (cps) ranging between 81 and 104. Intervals with low GR are few, restricted, and likely associated with the presence of fractures and/or thin sandstone layers. The highest GR values are almost exclusively associated with the marly layers that dominate the Marnoso–Arenacea Fm. (TSM03, TSM04, and TSM06) and the Schlier Fm. (TSM05).

P- (Vp) and S-wave (Vs) velocities obtained from the full-waveform sonic log were measured in the open-hole section down to the bottom of the hole, showing a wide range of values between different boreholes: Vp varies between 2972 and 5324 $m\,s^{-1}$ and Vs between 1800 and 2884 $m\,s^{-1}$ (Table 1; Figs. 6–9). Higher values were recorded along the boreholes that intersected more competent lithologies, especially limestones as for the Maiolica Fm. in TSM01 and Scaglia Rossa in TSM02. A significant decrease in both Vp and Vs was

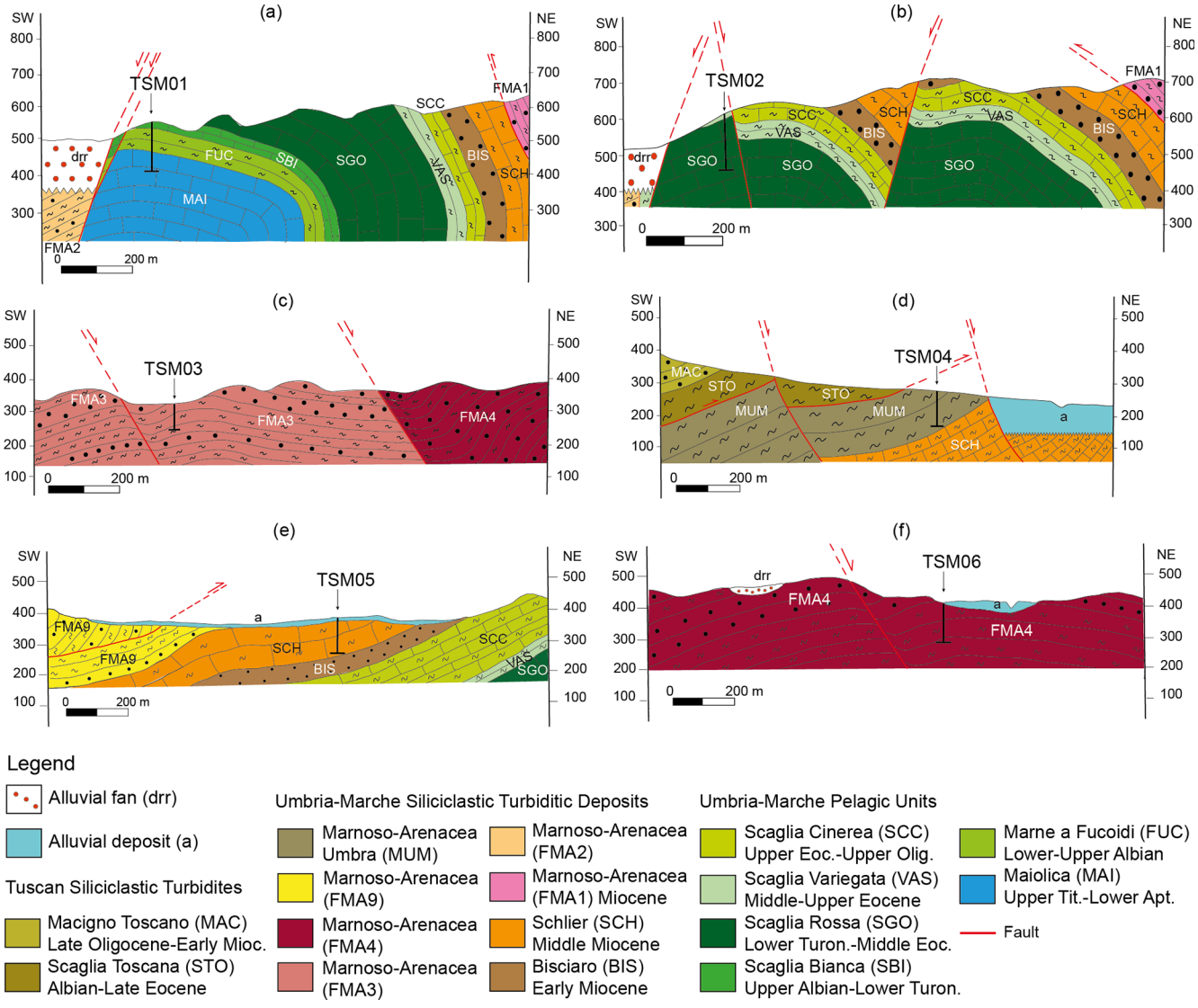

Figure 4. Geological cross-sections across the STAR boreholes. Different members of the Marnoso–Arenacea Fm. are shown (FMA1, 2, 3, 4, and 9 and MUM).

detected at open fracture occurrences. The dynamic Poisson ratio was computed using the specific formula from shear and compressional wave velocities from sonic logs to compare it to the fracture porosity. As expected, rocks with a low Poisson's ratio show a higher fracture density (Figs. 6–9).

Resistivity was measured in TSM03, TSM04, TSM05, and TSM06 boreholes. The values vary from 9 to 29 Ω m according to the response of sonic logs and fracture presence (Table 1); however, with the same lithology the resistivity values vary following the variations of single-point resistance (SPR).

Temperature measured in the boreholes (Table 1) is quite constant within a range of 12 to 18 °C, reflecting the borehole fluid rather than the "formation temperature". Due to the shallow investigated depth, the results are not very significant. See Sect. 3 for details.

Conductivity of the drilling fluid is directly proportional to the concentration of dissolved minerals and thus to its salinity: the highest values (694 $\mu S\,cm^{-1}$) were found in the TSM04 borehole near the area with intense CO_2 emissions of deep origin (Table 1).

4.3 Structure analysis

In this section we present the analysis of optical and acoustic images to identify the main discontinuities along the boreholes (Figs. 6–9). As mentioned before, we have grouped the features into six categories: open (in red), filled (in gray), bedding (in green), stylolite (in turquoise), chert layer (in dark gray), and weak zones. The filled and open fractures

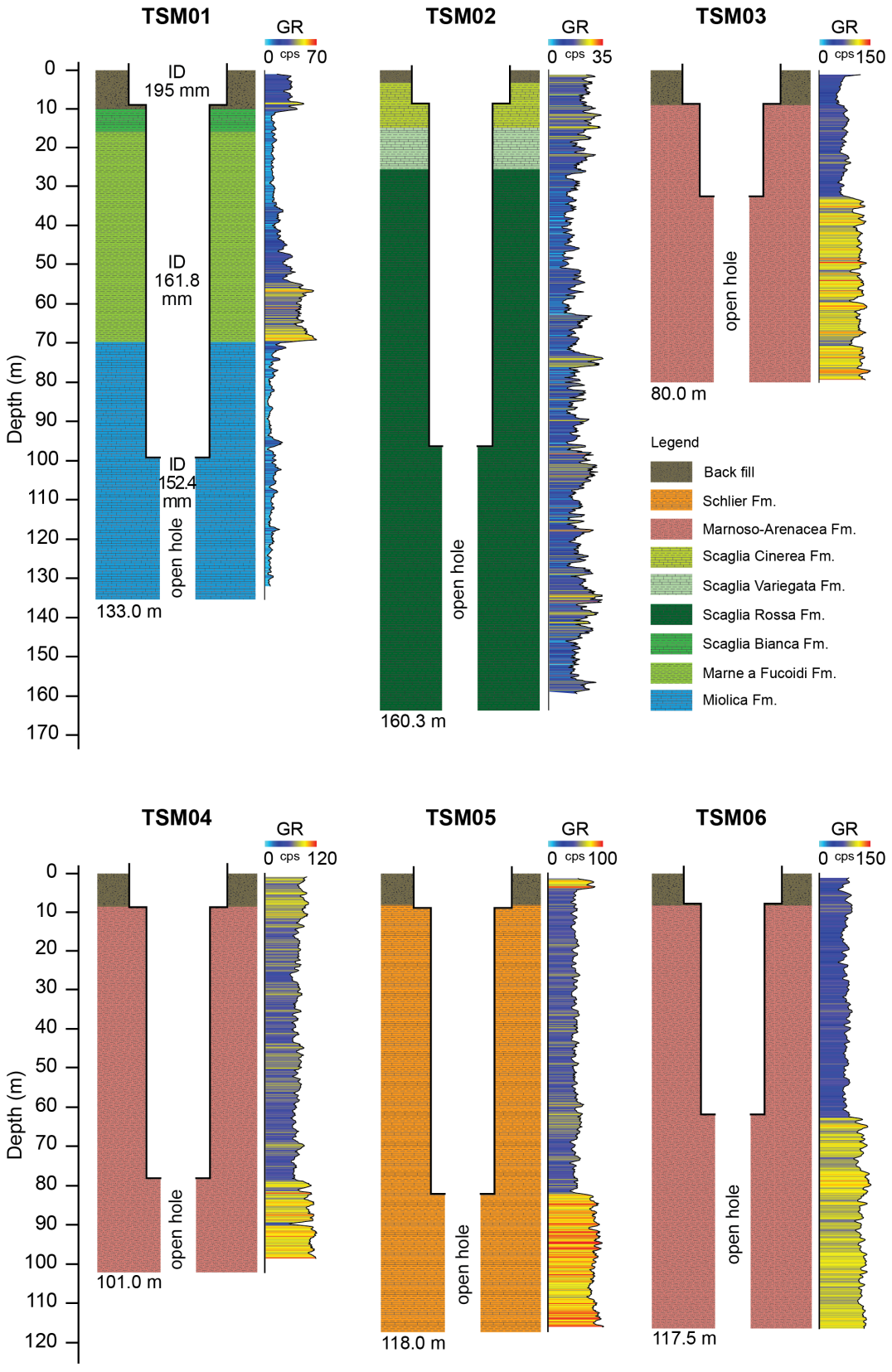

Figure 5. STAR boreholes with lithostratigraphic profile and gamma-ray log. Each borehole has a conductor casing for the first 9 m, followed by a casing and an open-hole section. ID: inner diameter. Only the total gamma (GR; unit: cps – counts per second) was also run through the casing, while all other measurements were performed only in the open hole. Seismometers and strainmeters were deployed at the bottom of the open section of each borehole (for details see Fig. S1 in the Supplement).

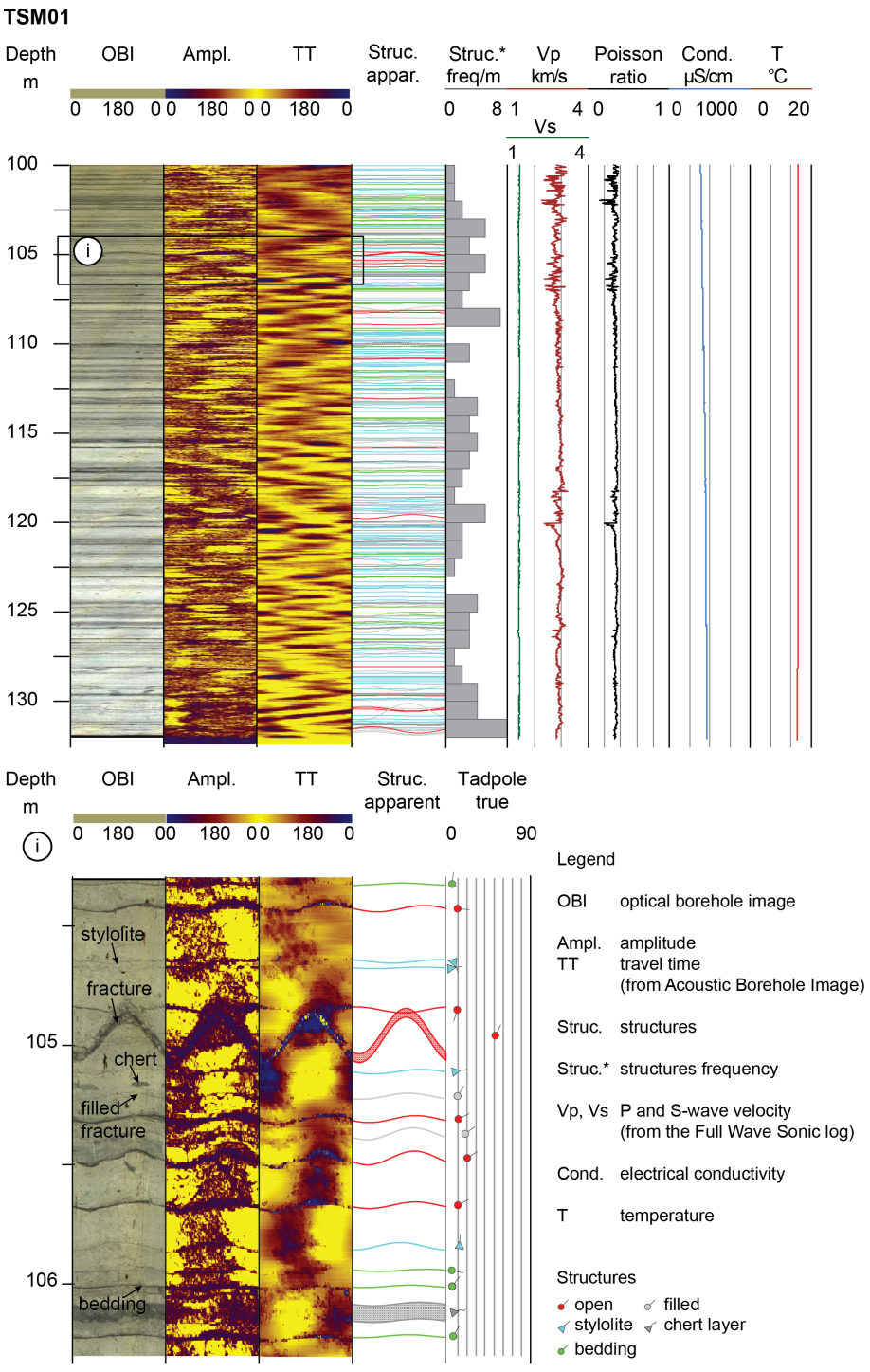

Figure 6. Downhole logging measurements performed along the TSM01 borehole (Maiolica Fm.). At the bottom: a detail of the structures intersected by the borehole.

usually have a thickness from a few millimeters up to 1–2 cm. Furthermore, we plotted the main tectonic structures (open and filled fractures and weak zones) as rose diagrams, splitting the data according to their dip (> and < 45°).

TSM01. The analysis of OBI and ABI images allowed us to identify and detect the main discontinuities crossed by the borehole (Fig. 6). The sub-horizontal discontinuities correspond to bedding planes, while the filled discontinuities can be interpreted as later-filled fractures or cleavage planes.

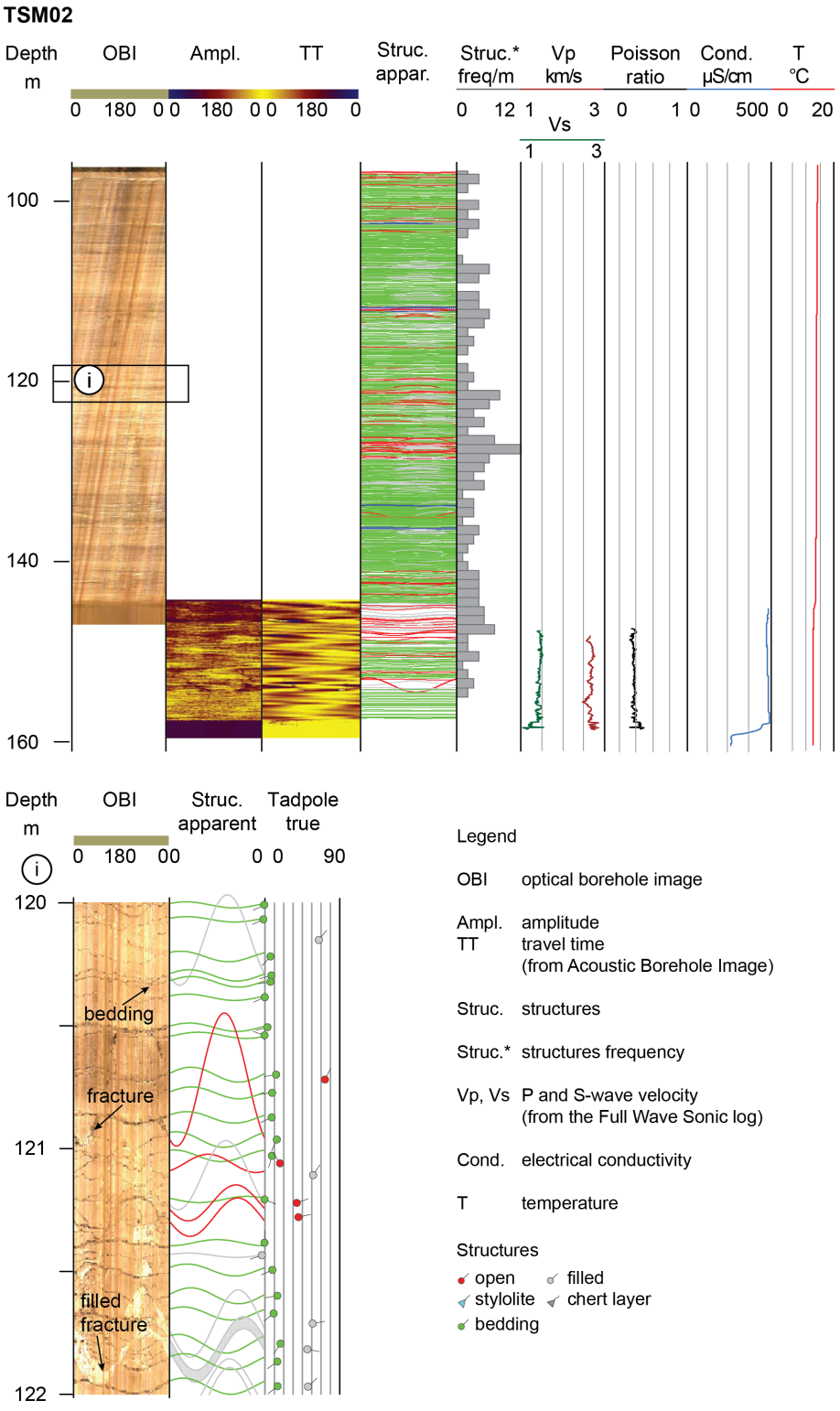

Figure 7. Downhole logging measurements performed along the TSM02 borehole (Scaglia Rossa Fm.). At the bottom: a detail of the structures intersected by the borehole.

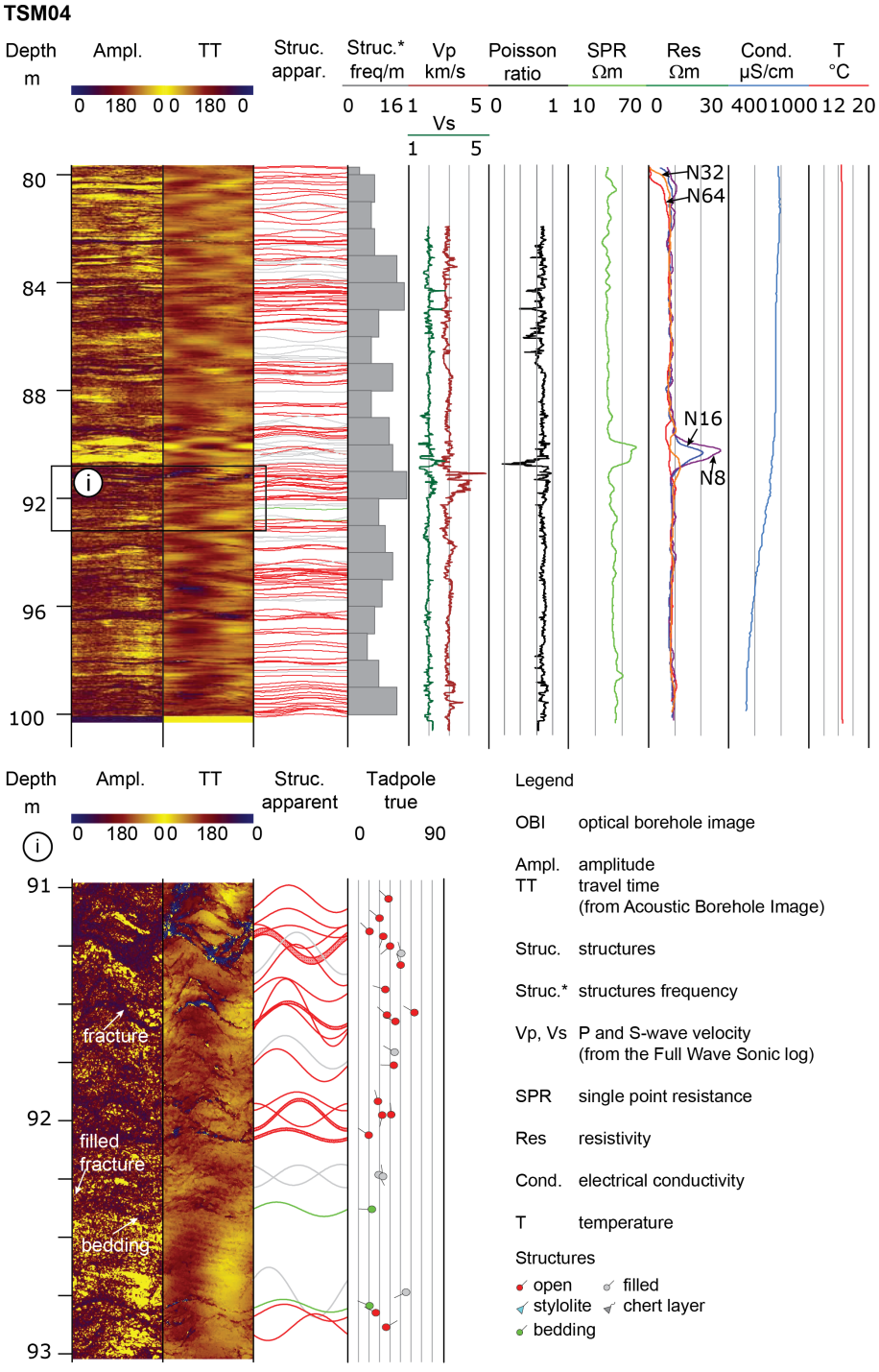

Figure 8. Downhole logging measurements performed along the TSM04 borehole (Marnoso–Arenacea Fm.). At the bottom: a detail of the structures intersected by the borehole. N means normal resistivity. The numbers (8, 16, 32, and 64) indicate the distance in inches between the electrode reference measuring point and the injection electrode in the resistivity sonde.

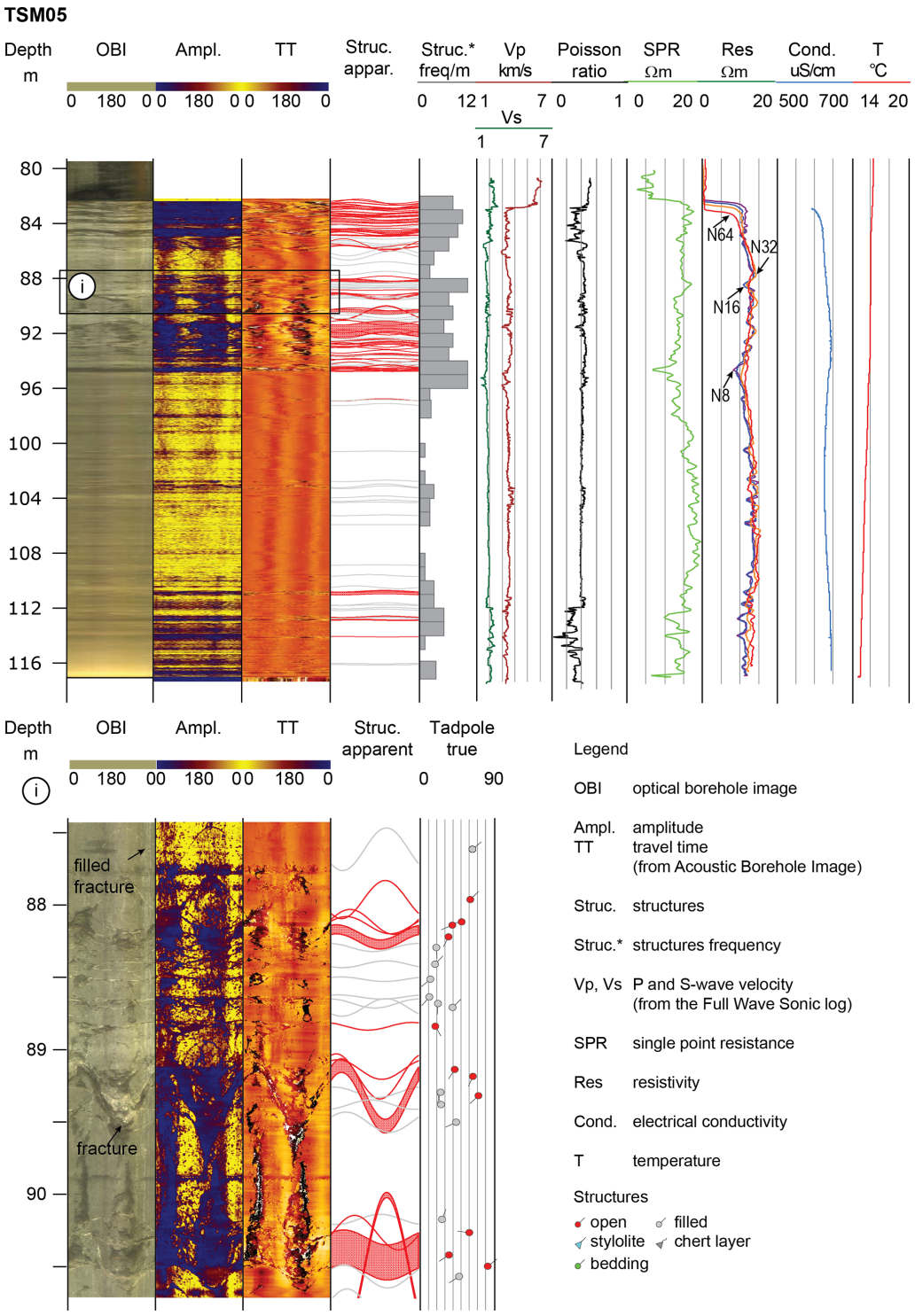

Figure 9. Downhole logging measurements performed along the TSM05 borehole (Schlier Fm.). At the bottom: a detail of the structures intersected by the borehole. N means normal resistivity. The numbers (8, 16, 32, and 64) indicate the distance in inches between the electrode reference measuring point and the injection electrode in the resistivity sonde.

Table 1. Geophysical properties of the rocks for TSM boreholes. GR: gamma ray (counts per second); Vp and Vs: P- and S-wave velocity, respectively; RES: resistivity; SPR: single-point resistance; *T*: temperature; COND: conductivity; CH: cased hole; OH: open hole. *The lithological formations refer to the open-hole section. Note that n.d. stands for no data.

Boreholes	ICDP ID	Lithological formation*	Depth m		GR cps		Vp $m s^{-1}$	Vs $m s^{-1}$	RES Ω m	SPR Ω m	*T* °C	COND $\mu S cm^{-1}$
			CH	OH	CH	OH						
TSM01	5070_1_A	Maiolica	0.0–99.3	99.3–133.0	17.9 ± 13.3	8.4 ± 4.4	5324 ± 371	2885 ± 112	n.d.	n.d.	12 ± 1	381 ± 40
TSM02	5070_2_A	Scaglia Rossa	0.0–97.0	97.0–160.3	11.7 ± 5.4	13.4 ± 5.6	4867 ± 184	2505 ± 500	n.d.	n.d.	15 ± 1	456 ± 62
TSM03	5070_3_B	Marnoso–Arenacea	0.0–32.0	32.0–80.0	61.5 ± 12.7	104.2 ± 15.9	3204 ± 168	1800 ± 130	29 ± 5	104 ± 10	14 ± 0.2	452 ± 7
TSM04	5070_4_A	Marnoso–Arenacea	0.0–79.3	79.3–101.0	61.5 ± 10.0	85.1 ± 13.2	2972 ± 207	1993 ± 118	9 ± 1	42 ± 5	16 ± 0.3	694 ± 92
TSM05	5070_5_A	Schlier	0.0–82.3	82.3–118.0	48.6 ± 8.7	81.2 ± 9.3	3451 ± 160	1879 ± 148	12 ± 3	53 ± 7	17 ± 1	634 ± 8
TSM06	5070_6_A	Marnoso–Arenacea	0.0–80.0	80.0–117.5	62.4 ± 9.2	99.7 ± 9.35	3422 ± 306	1896 ± 119	18 ± 3	76 ± 9	18 ± 0.03	487 ± 34

Moreover, numerous stylolites and chert layers are present within the Maiolica Fm., both parallel to bedding. A detail of the main features is shown in the inset of Fig. 6i. A total of 69 discontinuities (only open and filled fractures) were recorded along the open-hole section, showing a homogeneous distribution along the borehole with a maximum of eight structures per meter. The preferential orientation is NW–SE, corresponding to a dip azimuth of N200° (Fig. 10). The dip of these planes is generally low (around 25°), contributing to the azimuthal dispersion of the data. However, some discontinuities with steeper dips (ranging from 60 to 80°) are still NW–SE-oriented.

TSM02. The OBI and ABI images available for structural analysis investigated two different depth ranges. The OBI was performed from 96.2 to 147.0 m and the ABI from 144.2 to 159.6 m. The OBI image clearly shows continuous and parallel layering, especially interlayering of thin clay layers in the limestone. The Scaglia Rossa Fm. is also affected by numerous thick filled and open fractures. The analysis of the planar discontinuities identified on both images allowed us to distinguish bedding planes and filled and open fractures (Fig. 7). The latter two structures (195 counts) revealed a predominant orientation of NNW–SSE, corresponding to a dip azimuth of N204 (Fig. 10), with an average structure frequency of six per meter and a high discontinuity concentration around 120 to 125 m (Fig. 7i). The majority of open and filled fractures have dipping values higher than 45°, with the open ones dipping almost exclusively to the NE and the closed ones to the SW (Fig. 10).

TSM03. The poor quality of the OBI and ABI images made it difficult to perform a successful structural analysis. The unclear images are related to the high turbidity of the fluid in the borehole due to non-flushing of the borehole prior to acquisition and the high speed of running the OBI and ABI probes. Only the bedding planes were recognized, showing a mean orientation of NW–SE (dip azimuth of N201) with a very low dip of 11°. Owing to the low quality of the images, a geological survey was performed to measure bedding and main tectonic structures directly on the Marnoso–Arenacea outcrop near the drilling site (Fig. S2). Bedding varies from N204 near the borehole to N167 and N155, dipping about 5–15° W, consistent with what was observed from the data analysis along the borehole. The thickness of the sandstone levels of Marnoso–Arenacea Fm. is up to 100–120 cm, while the thickness of the gray marly layers ranges from 1 to 10 cm; they are laminated with cleavage planes subparallel to the bedding. There are fractures and sometimes sub-vertical faults, which are clearly visible in the sandstone layers, with an average fracture orientation of N050 subvertical, N215 sub-vertical faults with extensional displacement, and N213 dipping 76° W with left-lateral striae overlapped with oblique striae (pitch 55°; Fig. S2).

TSM04. The borehole intersected numerous discontinuity planes along the entire length of the measured log (Fig. 8). Although the log length is only approximately 20 m (79.8 to

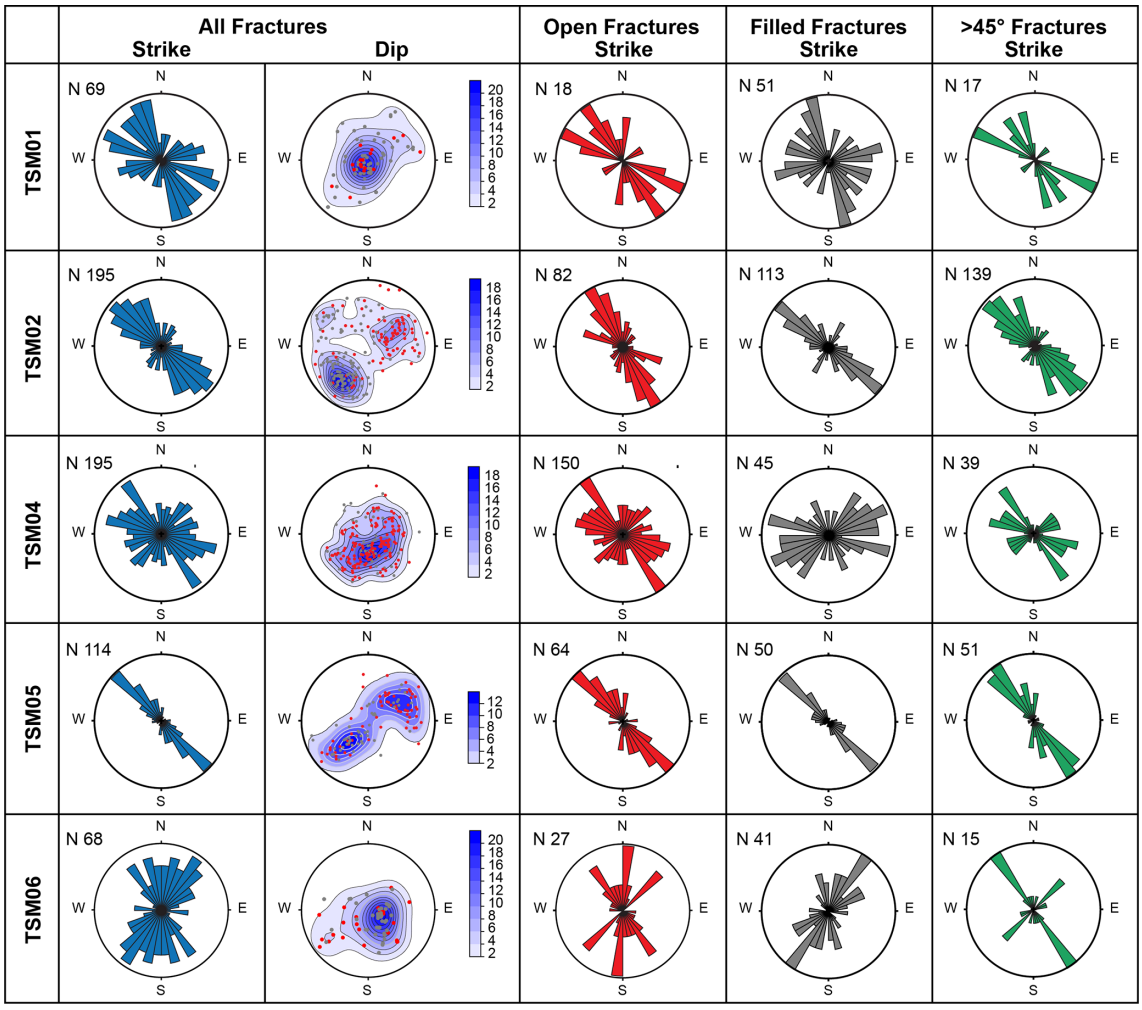

Figure 10. Rose diagrams and polar projections related to open and filled structures detected along the STAR boreholes (except TSM03). N: number of structures; DIP: poles of the planes (lower hemisphere) with the contouring (in percentage). The last column represents the fractures dipping > 45°.

100 m), the quality of the ABI images is significantly better compared to the TSM03 and TSM06 boreholes drilled in the same formation (Marnoso–Arenacea Fm.). The drastic decrease in cloudy fluid in the borehole is the combined result of wellbore flushing operations before starting log acquisition and the low running speed of the ABI probe, resulting in a good ABI image quality. A total of 195 discontinuities between filled and open fractures have been detected in the image log with an average orientation of N184 and dip never exceeding 60° (Fig. 10). In the field, upstream of the drilling site (Fig. S2), it was possible to measure bedding that is N180-oriented and dipping 25° W, related to a small Late Cretaceous–Early Miocene outcrop of Tuscan turbidites (Fig. 2).

TSM05. Analysis of OBI and ABI images allowed us to clearly identify tectonic structures such as open and filled structures (Fig. 9). The bedding planes are instead dubious and difficult to recognize. Discontinuity planes show a spacing that is quite dense (12 planes per 1 m) up to 94.8 m; below, they are very sparse, with sections of up to 3 m without discontinuity, probably also due to the acquisition and to the presence of cloudy drilling fluid in the borehole. From the image analysis a total of 114 planar structures have been identified with very consistent NW–SE orientation (corresponding to a dip azimuth of N219; Fig. 10). From this dataset, we have marked at least four different categories of discontinuity according to their dip, the presence or absence of filling, and their aperture. The first category of discontinuities is characterized by dip greater than 45°, which is related to both open and filled fractures. They show planes approximately NW–SE-oriented with dip towards both SW and NE. The filled fractures with dip less than 45° show a similar NW–SE trend, and the open fracture zones including wider zones (decimeter thicknesses up to 1 m; Fig. 9i) still have a NW–SE orientation and dips ranging from very low to almost vertical. The bedding planes are mainly sub-horizontal.

TSM06. The structural analysis has been performed only for the ABI image log, allowing us to identify 68 planar structures, 27 of which are open and 41 of which are filled in the Marnoso–Arenacea Fm. (Fig. 10). The planar discontinuities show a prevailing NE–SW orientation and dip 20–30° W. There is also a minor NNW–SSE-oriented data concentration characterized by steeper dip up to 60° NE. A weak zone oriented N300 dipping 54° NE with a width of about 21 cm has also been identified along the TSM06 borehole. In the field very close to the drilling site, bedding is N190-oriented, dipping 30° W. In the surroundings, low-angle bedding planes are also NW- and NE-oriented. Fracture planes are N125-oriented, dipping 88° S close to the drill; other high-angle tectonic structures are also E–W and NE–SW (Fig. S2).

5 Discussion and conclusion

In the framework of the STAR project, six shallow boreholes were drilled to create accurate geophysical downhole logs, aimed at identifying the most suitable depth in each borehole for the deployment of seismometers and strainmeters. The results of the seismometer and strainmeter network will require more time to obtain useful information for the project itself, dedicated to the study of the brittle upper crust and the structure and behavior of the Alto Tiberina low-angle seismogenic normal fault, in particular. This paper pertains solely to the initial phase of the STAR project, specifically focusing on the analysis of downhole geophysical well logs.

Downhole logging was the only way to characterize the borehole section, allowing the physical and structural properties of each geological formation to be determined, due to the lack of core samples. These in situ measurements are sensitive to formation properties on a scale that is intermediate between those obtained from literature data analysis performed on core or outcrop samples and deep geophysical measurements performed by exploration and production drilling companies. Most geophysical and petrophysical data available in the literature come from rock samples analyzed in laboratories or from well logs acquired along deep wells, whereas our data from geophysical logging of shallow boreholes provide an almost untapped source of information.

5.1 Physical properties

Regarding the calcareous formations of the Maiolica and Scaglia Rossa Fms., crossed by the boreholes TSM01 and TSM02, respectively, the physical properties of these competent rock types are well reflected by the acquired log data (Table 1), showing low average GR values (less than 18 cps) and relatively high average values of Vp (5.3 and 4.9 $\mathrm{km\,s^{-1}}$, respectively) and Vs (2.9 and 2.5 $\mathrm{km\,s^{-1}}$, respectively). The almost pure limestones of the Maiolica Fm. are characterized by lower GR and higher Vp and Vs values in comparison with the Scaglia Rossa Fm., where the clay content is significantly higher (up to 20 % in the Tertiary upper portion of the Scaglia Fm.; e.g., Arthur and Fischer, 1977).

The TSM03, TSM04, TSM05, and TSM06 boreholes were drilled in the marly intervals of the Neogene successions of the Marnoso–Arenacea Fm. and Schlier Fm. (TSM05). These clay-rich rocks are coherently characterized by high average GR (between 81 cps in the Schlier Fm. and 104 cps in the Marnoso–Arenacea Fm.; TSM03) and low RES (between 9 and 29 Ω m). The measurements include lower values for TSM04 (9 Ω m) and TSM05 (12 Ω m) at Marnoso–Arenacea and Schlier, respectively, intermediate values for TSM06 (18 Ω m), and higher values (up to 29 Ω m) for TSM03.

In greater detail, the average values are not totally representative of these complex formations, typically consisting of alternated marls and sandstones: a similar suggestion is derived from the relatively low Vp (3.0 to 3.5 $\mathrm{km\,s^{-1}}$) and Vs (1.8 to $\sim$ 2.0 $\mathrm{km\,s^{-1}}$) values. The temperature recorded in the boreholes (Table 1) is rather constant, with values between 12 and 18 °C, without showing any significant variations related to, e.g., outflow or inflow zones. Unfortunately, the shallow depth of the investigation limits the significance of the results.

We compared our RES results with data for two deep wells (San Donato 1 and Mt. Civitello 1 wells; https://www.videpi.com, last access: 20 August 2024) drilled in the same formations and considering the same analyzed depth interval, showing similar values between 20 and 30 Ω m for the Marnoso–Arenacea Fm. (Fig. S3). We have also investigated the resistivity of the Schlier Fm. along the Canopo 1 well (https://www.videpi.com, last access: 20 August 2024), although the latter is located far away from the study area, approximately 80 km NNE of Gubbio. Also in this case the resistivity values, around 7 Ω m, are comparable with our data (Fig. S3).

Information obtained from the velocity logs is more significant when including all six boreholes. We compared the Vp values recorded in the six shallow STAR boreholes (depth < 0.2 km; see Table 1) with data derived from sonic log analyses in much deeper wells (depth > 4 km) drilled in the same region for industrial purposes (Bigi et al., 2011; Scisciani et al., 2014; Montone and Mariucci, 2020; Trippetta et al., 2021). These studies report average Vp values between 4.0 and 4.8 $\mathrm{km\,s^{-1}}$ for the Marnoso–Arenacea Fm., 4.4 to 4.8 $\mathrm{km\,s^{-1}}$ for the Schlier Fm., 5.3 to 5.8 $\mathrm{km\,s^{-1}}$ for the Scaglia Rossa Fm., and 5.5 to 6.1 $\mathrm{km\,s^{-1}}$ for the Maiolica Fm. All these values are approximately 15 % higher than our results but follow the same overall trend, with higher average Vp values recorded in the Maiolica Fm. and lower values in the Tertiary marly formations. This increase in P-wave velocity with depth is primarily attributed to increased rock density and compaction, particularly in the Tertiary formations.

Due to a different degree of porosity linked to the different investigated depths and to the pore type, P-wave velocity can significantly change (e.g., Hairabian et al., 2014;

Smeraglia et al., 2014; Trippetta et al., 2021). Moreover, P-wave velocity also depends on factors such as lithology changes, presence of fractures or faults, and also the different amount of tectonic deformation observed in different structural domains (Trippetta et al., 2021). The process of collecting and analyzing velocity data on upper-crustal sedimentary rocks is very useful for several reasons. On one hand, these values help build and calibrate more accurate 2D and 3D velocity models that can be used to improve earthquake localization (e.g., Latorre et al., 2016; Montone and Mariucci, 2023) as well as to constrain depth conversion of seismic reflection profiles. On the other hand, since the velocity parameters of rocks are strictly related to their rigidity, velocity values also reflect their different mechanical behavior and may ultimately influence earthquake generation and distribution. In our case, the more competent carbonate formations (i.e., Maiolica and Scaglia Rossa Fms.) are characterized by systematically higher velocities compared to less competent, clay-rich turbidite formations (i.e., Schlier and Marnoso–Arenacea Fms.).

In the ATF region, as well as in adjacent areas in the same seismotectonic framework of the central Apennines, several recent studies of the relationships between seismicity distribution and upper-crustal geological setting have been recently performed by plotting accurately relocated seismic sequences on well-calibrated geological subsurface models based on depth conversion of seismic reflection profiles (e.g., Latorre et al., 2016; Barchi et al., 2021; Collettini et al., 2022; Chiaraluce et al., 2017a). These studies coherently indicated that upper-crustal seismicity (and the normal-faulting earthquake main shocks, in particular) is systematically hosted in the high-velocity Mesozoic or early Tertiary successions, consisting of carbonates, dolostones, and anhydrites, whilst only a few low-magnitude events are recorded in the overlying, less competent Neogene turbidites, mainly consisting of marls and sandstones.

5.2 Stress field

To constrain the orientation of the stress field in the area of the STAR project, we have analyzed and interpreted the fractures detected in the six boreholes and compared them with the breakout orientations from two deep wells and also with the other stress indicators, mainly focal mechanism data. In our boreholes, ABI and OBI images do not reveal any borehole breakouts. However, breakouts at very shallow depth could not be related to or representative of the stress field because their occurrence would be linked to local effects such as topography, local faulting, folding, and other near-surface geological structures. As already mentioned, in the STAR study area (Fig. 2) two deep wells (SD and MC) were drilled in the past, reaching depths of 4763 and 5600 m, respectively. The SD well is located very close to the ATF, intersecting it at a shallow depth, while the MC well, approximately 15 km east of the ATF, intersects additional tectonic structures. A thorough analysis of borehole breakout stress data collected along the two deep wells allowed us to deduce the current stress field orientation (Mariucci et al., 2008). In the case of the SD well, the borehole breakout results reveal a minimum horizontal stress orientation of N055 $\pm$ 22°; the MC well exhibits a slightly different stress orientation, with a value of N012 $\pm$ 29° (Fig. 11).

To interpret the structural data obtained along the STAR boreholes, we have considered (i) the shallow depth of the boreholes, (ii) their near-vertical inclination that strongly underestimates the occurrence of near-vertical features (Terzaghi, 1965; Massiot et al., 2015), and (iii) the difficulty in distinguishing fractures from faults in these types of data.

Along the STAR boreholes, the main features with a dip angle $> 45°$ (Fig. 10) show a predominantly NW–SE orientation and could be interpreted as pre-existing fractures generated in the early phases of the deformation history before folding (Price, 1966).

Considering that the current stress field in the area is primarily due to an extensional regime, with the main compressional stress as well as sigma 1 and the vertical and horizontal sigma 3 NE–SW-oriented, the tectonic structures associated with this latter stress field consequently develop normal faults and high-dip extensional fractures. These $> 45°$ NW–SE structures, favorably oriented with respect to the current extensional stress field (Fig. 11), might have been reactivated as extensional fractures. In TSM04 and TSM06 boreholes, for structures with a dip greater than 45° (Fig. 10), another orientation is also observed, approximately 90° from the previous one. We can assume that fractures oriented both NW–SE and NE–SW are contemporaneous and linked to the same extensional stress field, primarily guided by a vertical sigma 1. On the other hand, structures with low dip – still NW–SE-oriented – could be attributed to previous compressive deformation phases linked to a stress field characterized by a horizontal sigma 1, oriented NE–SW. Taking into careful consideration the different depths investigated by the STAR boreholes (< 0.2 km) with respect to the active stress data mainly inferred from breakout data in deep wells (0.5–6 km) and focal mechanisms of crustal earthquakes (usually 5–15 km), we can still compare their results (Fig. 11). In fact, most of the results from the literature on the orientation of the stress field have shown that different crustal depths do not reorient or change the stress field (Heidbach et al., 2016; Mariucci and Montone, 2024). An almost constant orientation of the minimum horizontal stress characterizes this sector of the Apennines, from the southern L'Aquila and Norcia zones to the areas north of Gubbio, showing only a slight rotation from ENE–NE directions to NE–NNE directions, respectively (Fig. 11). This is observed from numerous data derived from earthquake focal mechanisms as well as breakout data in deep wells, also present in the southernmost sector (Mariucci and Montone, 2016) and active fault data (Lavecchia et al., 2022), under a stress regime that can be defined as exclusively extensional.

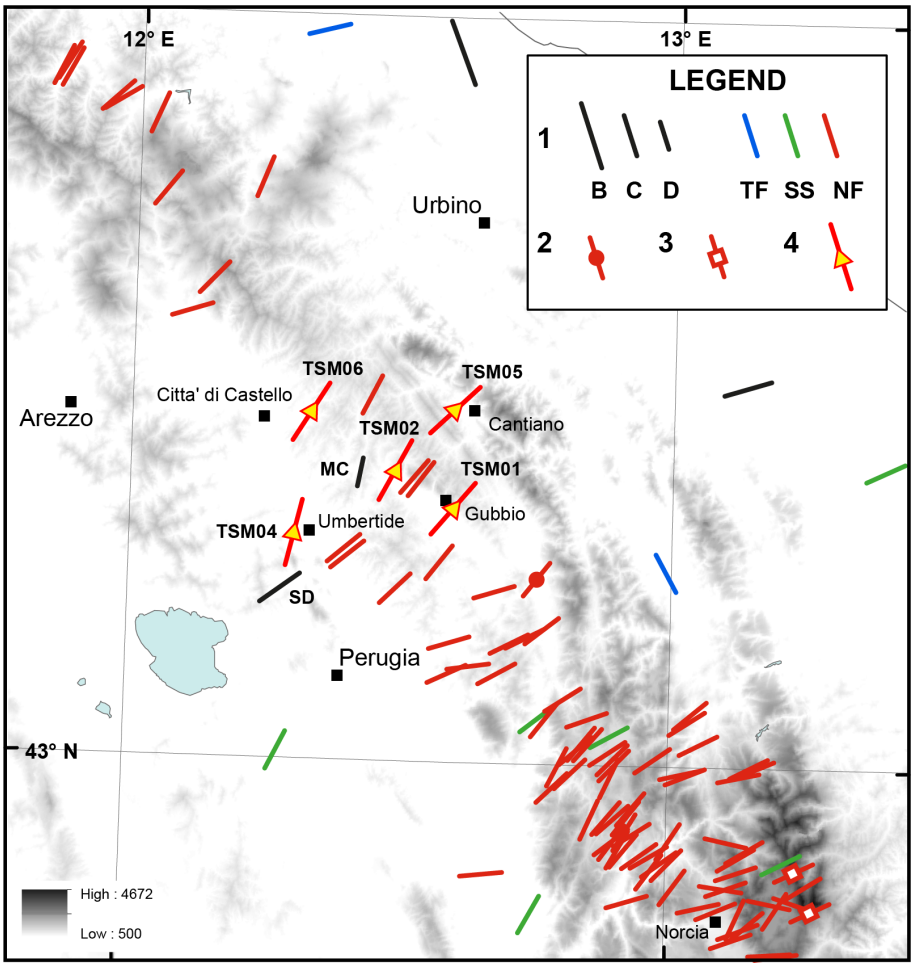

Figure 11. Present-day stress field of central Italy. The minimum horizontal stress orientations inferred from the $> 45°$ dipping fractures detected along the STAR boreholes (bars with yellow triangles) and from the Italian present-day stress indicator database (IPSI) 1.6 (Mariucci and Montone, 2024) are shown. 1 – Borehole breakout (black bar) and focal mechanism (colored bar) data; 2 – formal inversion data; 3 – fault data. All data are scaled by quality (from B to D) and colored according to tectonic regime: the black bar is an unknown regime (breakout), blue is thrust faulting, green is strike-slip faulting, and red is normal faulting. 4 – data from TSM boreholes.

In conclusion, our paper provides reliable values of physical properties of rocks, in particular P-wave velocity, which can be used to characterize crustal velocity models and allow detailed interpretation of seismic profiles when investigating the first 200 m of the crust. However, detailed geophysical measurements from shallow boreholes are relatively rare. A small, homogeneous rock sample analyzed in the laboratory may not accurately represent the complexity of the in situ rock formation, which can exhibit significant internal variability in composition and fracturing. Additionally, although our sites provide in situ measurements, they represent a relatively small dataset compared to the extensive data collected from deep well logs, which span hundreds of meters. This limitation could explain the discrepancies observed, such as the differences in Vp values. While our measured values are lower than the average data, they still fall within the acceptable range.

Beyond the specific case presented, our data significantly enhance our understanding of the upper crust. These in situ measurements bridge the gap between data from outcropping rocks and data from deeper wells. In particular, this scientific approach is able to provide useful geophysical information at a very shallow crustal depth (< 0.2 km) typically not explored by the scientific community or the oil and gas industry. Our study demonstrates that even a limited dataset can provide valuable insights and represent a possible case history for future projects. With an expanded dataset across a region of interest, it would be possible to illuminate a comprehensive section of the crust, extending from the surface to several kilometers deep and potentially even deeper.

Data availability. The downhole logging dataset and additional information about the boreholes are available from the ICDP repository database (https://www.icdp-online.org/projects/by-continent/europe/star-italy/public-data/, International Continental Scientific Drilling Program, 2024).

Supplement. The supplement related to this article is available online at: https://doi.org/10.5194/se-15-1385-2024-supplement.

Author contributions. PM, SP, MRB: conceptualization, methodology. PM, SP, MTM, AA: formal analysis. PM, SP, MTM, LC, MU, FM, WJ: field investigation. LC, AA, MU, FM: data curation. PM, SP, MRB, MTM: writing – original draft preparation. SP, MU, MTM: visualization. PM, SP, MRB, MTM: writing – review and editing. All co-authors contributed to reviewing and revising the paper. All authors have read and agreed to the published version of the manuscript.

Competing interests. The contact author has declared that none of the authors has any competing interests.

Disclaimer. Publisher's note: Copernicus Publications remains neutral with regard to jurisdictional claims made in the text, published maps, institutional affiliations, or any other geographical representation in this paper. While Copernicus Publications makes every effort to include appropriate place names, the final responsibility lies with the authors.

Acknowledgements. GEOTEC (http://geo-tec.it/en/, last access: 20 August 2024) and GEOLOGIN Srl (https://www.geolog-in.com/, last access: 20 August 2024) are thanked for providing drilling and geophysical borehole log data. We are grateful to Earthscope for providing strainmeters. We thank the United States National Science Foundation (NSF) and the INGV colleagues who worked on the implementation of the TABOO-NFO research infrastructure. Many thanks are due to Maria Beatrice Magnani, Giacomo Medici, and an anonymous reviewer, who improved the paper with useful comments and suggestions. Katja Heeschen (GFZ) is thanked for helping with database management.

Financial support. This research has been supported by the International Continental Scientific Drilling Program (ICDP-2018/05) and the European Research Council (ERC; grant agreement no. 835012, TECTONIC). In addition, this work would not have been possible without the contribution of the Istituto Nazionale di Geofisica e Vulcanologia.

Review statement. This paper was edited by Federico Rossetti and reviewed by Maria Beatrice Magnani and one anonymous referee.

References

Amato, A. and Cocco, M. (Eds.): The Umbria-Marche, central Italy, Seismic Sequence of 1997–1998, J. Seismol., 4, 5–598, 2000.

Amato, A., Azzara, R., Chiarabba, C., Cimini, G. B., Cocco, M., Di Bona, M., Margheriti, L., Mazza, S., Mele, F., Selvaggi, G., Basili, A., Boschi, E., Courboulex, F., Deschamps, A., Gaffet, S., Bittarelli, G., Chiaraluce, L., Piccinini, D., and Ripepe, M.: The 1997 Umbria-Marche seismic sequence: a first look at the main shocks and aftershocks, Geophys. Res. Lett., 25, 2861–2864, 1998.

Anderlini, L., Serpelloni, E., and Belardinelli, M.: Creep and locking of a low-angle normal fault: Insights from the Altotiberina fault in the Northern Apennines (Italy), Geophys. Res. Lett., 43, 4321–4329, https://doi.org/10.1002/2016GL068604, 2016.

Arthur, M. A. and Fischer, A. G.: Upper Cretaceous-Paleocene magnetic stratigraphy at Gubbio, Italy I. Lithostratigraphy and sedimentology, Geol. Soc. Am. Bull., 88, 367–371, 1977.

Barchi, M. R.: The Neogene-Quaternary evolution of the Northern Apennines: crustal structure, style of deformation and seismicity, Journal of the Virtual Explorer, 36, 11, https://doi.org/10.3809/jvirtex.2010.00220, 2010.

Barchi, M. R. and Collettini, C.: Seismicity of central Italy in the context of the geological history of the Umbria-Marche Apennines, Special Paper of the Geological Society of America, 542, 175–190, 2019.

Barchi, M. R. and Mirabella, F.: The 1997–98 Umbria-Marche earthquake sequence: "Geological" vs. "seismological" faults, Tectonophysics, 476, 170–179, https://doi.org/10.1016/j.tecto.2008.09.013, 2009.

Barchi, M. R., De Feyter, A., Magnani, M. B., Minelli, G., Pialli, G., and Sotera, B. M.: The structural style of the Umbria-Marche fold and thrust belt, Memorie della Societá Geologica Italiana, 52, 557–578, 1998.

Barchi, M. R., Carboni, F., Michele, M., Ercoli, M., Giorgetti, C., Porreca, M., Azzaro, S., and Chiaraluce, L.: The influence of subsurface geology on the distribution of earthquakes during the 2016–2017 Central Italy seismic sequence, Tectonophysics, 807, 22879, https://doi.org/10.1016/j.tecto.2021.228797, 2021.

Bigi, S., Casero, P., and Ciotoli, G.: Seismic interpretation of the Laga basin; constraints on the structural setting and kinematics of the Central Apennines, J. Geol. Soc. London, 168, 179–190, https://doi.org/10.1144/0016-76492010-084, 2011.

Bohnhoff, M., Dresen, G., Ceken, U., Kadirioglu, F. T., Kartal, R. F., Kilic, T., Nurlu, M., Yanik, K., Acarel, D., Bulut, F., Ito, H., Johnson, W., Malin, P. E., and Mencin, D.: GONAF – the borehole Geophysical Observatory at the North Anatolian Fault in the eastern Sea of Marmara, Sci. Dril., 22, 19–28, https://doi.org/10.5194/sd-22-19-2017, 2017.

Boncio, P. and Lavecchia, G.: A geological model for the Colfiorito earthquakes (September–October 1997, central Italy), J. Seismol., 4, 345–356, 2000.

Boncio, P., Pizzi, A., Brozzetti, F., Pomposo, G. Lavecchia, G., Di Naccio, D., and Ferrarini, F.: Coseismic ground deformation of the 6 April 2009 L'Aquila earthquake (central Italy, M_w 6.3), Geophys. Res. Lett., 37, L06308, https://doi.org/10.1029/2010GL042807, 2010.

Caricchi, C., Aldega, L., Barchi, M. R., Corrado, S., Grigo, D., Mirabella, F., and Zattin, M.: Exhumation patterns along shallow low-angle normal faults: an example from the Altotiberina

active fault system (Northern Apennines, Italy), Terra Nova, 27, 312–321, https://doi.org/10.1111/ter.12163, 2015.

Cello, G., Mazzoli, S., Tondi, E., and Turco, E.: Active tectonics in the central Apennines and possible implications for seismic hazard analysis in peninsular Italy, Tectonophysics, 272, 43–68, https://doi.org/10.1016/S0040-1951(96)00275-2, 1997.

Chiarabba, C., Jovane, L., and Di Stefano, R.: A new view of Italian seismicity using 20 years of instrumental recordings, Tectonophysics, 305, 251–268, 2005.

Chiarabba, C., De Gori, P., Cattaneo, M., Spallarossa, D., and Segou, M.: Faults geometry and the role of fluids in the 2016–2017 Central Italy seismic sequence, Geophys. Res. Lett., 45, 6963–6971, https://doi.org/10.1029/2018GL077485, 2018.

Chiaraluce, L., Ellsworth, W. L., Chiarabba, C., and Cocco, M.: Imaging the complexity of an active normal fault system: The 1997 Colfiorito (Central Italy) case study, J. Geophys. Res., 108, 2294, https://doi.org/10.1029/2002JB002166, 2003.

Chiaraluce, L., Amato, A., Carannante, S., Castelli, V., Cattaneo, M., Cocco, M., Collettini, C., D'Alema, E., Di Stefano, R., Latorre, D., Marzorati, S., Mirabella, F., Monachesi, G., Piccinini, D., Nardi, A., Piersanti, A., Stramondo, S., and Valoroso, L.: The Alto Tiberina Near Fault Observatory (northern Apennines, Italy), Ann. Geophys., 57, S0327, https://doi.org/10.4401/ag-6426, 2014a.

Chiaraluce, L., Collettini, C., Cattaneo, M., and Monachesi, G.: The shallow boreholes at The AltotiBerina near fault Observatory (TABOO; northern Apennines of Italy), Sci. Dril., 17, 31–35, https://doi.org/10.5194/sd-17-31-2014, 2014b.

Chiaraluce, L., Di Stefano, R., Tinti, E., Scognamiglio, L., Michele, M., Casarotti, E., Cattaneo, M., De Gori, P., Chiarabba, C., Monachesi, G., Lombardi, A., Valoroso, L., Latorre, D., and Marzorati, S.: The 2016 Central Italy seismic sequence: a first look at the mainshocks, aftershocks, and source models, Seismol. Res. Lett., 88, 757–771, https://doi.org/10.1785/0220160221, 2017a.

Chiaraluce, L., Festa, G., Bernard, P., Caracausi, A., Carluccio, I., Clinton, J. F., Di Stefano, R., Elia, L., Evangelidis, C. P., Ergintav, S., Jianu, O., Kaviris, G., Marmureanu, A., Šebela, S., and Sokos, E.: The role of rheology, crustal structures and lithology in the seismicity distribution of the northern Apennines, Tectonophysics, 694, 280–291, https://doi.org/10.1016/j.tecto.2016.11.011, 2017b.

Chiaraluce, L., Festa, G., Bernard, P., Caracausi, A., Carliccio, I., Clinton, J., Di Stefano, R., Elia, L., Evangelidis, C., Ergintav, S., Jianu, O., Kaviris, G., Marmureanu, A., Sebela., S., and Sokos, E.: The Near Fault Observatory community in Europe: a new resource for faulting and hazard studies, Ann. Geophys., 65, DM316, https://doi.org/10.4401/ag-8778, 2022.

Chiaraluce, L., Bennett, R., Mencin, D., Johnson, W., Barchi, M. R., Bohnhoff, M., Baccheschi, P., Caracausi, A., Calamita, C., Cavaliere, A., Gualandi, A., Mandler, E., Mariucci, M. T., Martelli, L., Marzorati, S., Montone, P., Pantaleo, D., Pucci, S., Serpelloni, E., Supino, M., Stramondo, S., Hanagan, C., Van Boskirk, L., Gottlieb, M., Mattioli, G., Urbani, M., Mirabella, F., Akimbekova, A., Pierdominici, S., Wiersberg, T., Marone, C., Palmieri, L., and Schenato, L.: A strainmeter array as the fulcrum of novel observatory sites along the Alto Tiberina Near Fault Observatory, Sci. Dril., 33, 173–190, https://doi.org/10.5194/sd-33-173-2024, 2024.

Ciaccio, M. G., Barchi, M. R., Chiarabba, C., Mirabella, F., and Stucchi, E.: Seismological, geological and geophysical constraints for the Gualdo Tadino fault, Umbria–Marche Apennines (central Italy), Tectonophysics, 406, 233–247, https://doi.org/10.1016/j.tecto.2005.05.027, 2005.

Cinti, F. R., Cucci, L., Marra, F., and Montone, P.: The 1997 Umbria-Marche (Italy) earthquake sequence: Relationship between ground deformation and seismogenic structure, Geophys. Res. Lett., 26, 895–898, 1999.

Collettini, C., Barchi, M. R., De Paola, N., Trippetta, F., and Tinti, E.: Rock and fault rheology explain differences between on fault and distributed seismicity, Nat. Commun., 13, 5627, https://doi.org/10.1038/s41467-022-33373-y, 2022.

Cresta, S., Monechi, S., and Parisi, G.: Stratigrafia del Mesozoico al Cenozoico nell'area Umbro-Marchigiana, Memorie Descrittive della Carta Geologica d'Italia, Istituto Poligrafico e Zecca dello Stato, Roma, Italia, 185 pp., ISBN 978-88-240-2295-5, 1989.

Davatzes, N. C. and Hickman, S. H.: Stress, fracture, and fluid-flow analysis using acoustic and electrical image logs in hot fractured granites of the Coso geothermal field, California, U. S. A., in: Dipmeter and borehole image log technology, edited by: Poppelreiter, M., Garcia-Carballido, C., and Kraaijveld, M., AAPG Memoir., 92, 259–293, 2010.

De Paola, N., Faulkner, D. R., and Collettini, C.: Brittle versus ductile deformation as the main control on the transport properties of low-porosity anhydrite rocks, J. Geophys. Res., 114, B06211, https://doi.org/10.1029/2008JB005967, 2009.

Deschamps, A., Iannaccone, G., and Scarpa, R.: The Umbrian earthquake (Italy) of 19 September 1979, Ann. Geophys., 2, 29–36, 1984.

Diaferia, I., Barchi, M., Loddo, M., Schiavone, D., and Siniscalchi, A.: Detailed imaging of tectonic structures by multiscale Earth resistivity tomographies: The Colfiorito normal faults (central Italy), Geophys. Res. Lett., 33, L09305, https://doi.org/10.1029/2006GL025828, 2006.

Ellis, D. V. and Singer, J. M.: Well Logging for Earth Scientists, in: 2nd Edn., Springer, 699 pp., ISBN 978-1-4020-3738-2, 2007.

EMERGEO Working Group: Evidence for surface rupture associated with the M_w 6.3 L'Aquila earthquake sequence of April 2009 (central Italy), Terra Nova, 22, 43–51, 2010.

Fischer, T., Hrubcová, P., Dahm, T., Woith, H., Vylita, T., Ohrnberger, M., Vlček, J., Horálek, J., Dědeček, P., Zimmer, M., Lipus, M. P., Pierdominici, S., Kallmeyer, J., Krüger, F., Hannemann, K., Korn, M., Kämpf, H., Reinsch, T., Klicpera, J., Vollmer, D., and Daskalopoulou, K.: ICDP drilling of the Eger Rift observatory: magmatic fluids driving the earthquake swarms and deep biosphere, Sci. Dril., 31, 31–49, https://doi.org/10.5194/sd-31-31-2022, 2022.

Haessler, H., Gaulon, R., Rivera, L., Console, R., Frogneux, M., Gasparini, G., Martel, L., Patau, G., Siciliano, M., and Cisternas, A.: The Perugia (Italy) earthquake of 29 April 1984: a microearthquake survey, B. Seismol. Soc. Am., 78, 1948–1964, 1988.

Hairabian, A., Fournier, F., Borgomano, J., and Nardon, S.: Depositional facies, pore types and elastic properties of deep-water gravity flow carbonates, J. Petrol. Geol., 37, 231–249, 2014.

Heidbach, O., Rajabi, M., Reiter, K., Ziegler, M., and WSM Team: World Stress Map Database Release 2016. V. 1.1, GFZ Data Services, https://doi.org/10.5880/WSM.2016.001, 2016.

International Continental Scientific Drilling Program: Public Data and Images, International Continental Scientific Drilling Program [data set], https://www.icdp-online.org/projects/by-continent/europe/star-italy/public-data/ (last access: 25 November 2024), 2024.

Langbein, J., Murray, J. R., and Snyder, H. A.: Coseismic and initial postseismic deformation from the 2004 Parkfield, California, earthquake, observed by Global Positioning System, electronic distance meter, creepmeters, and borehole strainmeters, B. Seismol. Soc. Am., 96, S304–S320, 2006.

Latorre, D., Mirabella, F., Chiaraluce, L., Trippetta, F., and Lomay, A.: Assessment of earthquake locations in 3-D deterministic velocity models: A case study from the Altotiberina Near Fault Observatory (Italy), J. Geophys. Res.-Sol. Ea., 121, 8113–8135, https://doi.org/10.1002/2016JB013170, 2016.

Lavecchia, G., Adinolfi, G. M., de Nardis, R., Ferrarini, F., Cirillo, D., Brozzetti, F., De Matteis, R., Festa, G., and Zollo, A.: Multidisciplinary inferences on a newly recognized active east-dipping extensional system in Central Italy, Terra Nova, 29, 77–89, 2017.

Lavecchia, G., Bello, S., Andrenacci, C., Cirillo, D., Ferrarini, F., Vicentini, N., de Nardis, R., Roberts, G., and Brozzetti, F.: Quaternary fault strain INdicators database – QUIN 1.0-first release from the Apennines of central Italy, Scientific Data, 9, 204, https://doi.org/10.1038/s41597-022-01311-8, 2022.

Mariucci, M. T. and Montone, P.: Contemporary stress field in the area of the 2016 Amatrice seismic sequence (central Italy), Ann. Geophys., 59, 5, https://doi.org/10.4401/ag-7235, 2016.

Mariucci, M. T. and Montone, P.: IPSI 1.6, Database of Italian Present-day Stress Indicators, Istituto Nazionale di Geofisica e Vulcanologia (INGV), https://doi.org/10.13127/IPSI.1.6, 2024.

Mariucci, M. T., Montone, P., and Pierdominici, S.: Active stress field in central Italy: a revision of deep well data in Umbria region, Ann. Geophys., 51, 433–442, 2008.

Marzorati, S., Massa, M., Cattaneo, M., Monachesi, G., and Frapiccini, M.: Very detailed seismic pattern and migration inferred from the April 2010 Pietralunga (northern Italian Apennines) micro-earthquake sequence, Tectonophysics, 610, 91–109, https://doi.org/10.1016/j.tecto.2013.10.014, 2014.

Massiot, C., McNamara, D., and Lewis, B.: Processing and analysis of high temperature geothermal acoustic borehole image logs in the Taupo Volcanic Zone, New Zealand, Geothermics, 53, 190–201, https://doi.org/10.1016/j.geothermics.2014.05.010, 2015.

Mcginnis, R. N., Ferrill, D. A., Morris, A. P., Smart, K. J., and Lehrmann, D.: Mechanical stratigraphic controls on natural fracture spacing and penetration, J. Struct. Geol., 95, 160–170, https://doi.org/10.1016/j.jsg.2017.01.001, 2017.

Medici, G., Ling, F., and Shang, J.: Review of discrete fracture network characterization for geothermal energy extraction, Front. Earth Sci., 11, 1328397, https://doi.org/10.3389/feart.2023.1328397, 2023.

Michele, M., Chiaraluce, L., Di Stefano, R., and Waldhauser, F.: Fine-Scale Structure of the 2016–2017 Central Italy Seismic Sequence From Data Recorded at the Italian National Network, J. Geophys. Res., 125, e2019JB01844, https://doi.org/10.1029/2019JB018440, 2020.

Mildon, Z. K., Roberts, G. P., Faure Walker, J. P., Wedmore, L. N. J., and McCaffrey, K. J. W.: Active normal faulting during the 1997 seismic sequence in Colfiorito, Umbria: Did slip propagate to the surface?, J. Struct. Geol., 91, 102–113, 2016.

Mirabella, F., Ciaccio, M. G., Barchi, M. R., and Merlini, S.: The Gubbio normal fault (Central Italy): geometry, displacement distribution and tectonic evolution, J. Struct. Geol., 26, 2233–2249, https://doi.org/10.1016/j.jsg.2004.06.009, 2004.

Mirabella, F., Brozzetti, F., Lupattelli, A., and Barchi, M. R.: Tectonic evolution of a low-angle extensional fault system from restored cross-sections in the Northern Apennines (Italy), Tectonics, 30, TC6002, https://doi.org/10.1029/2011TC002890, 2011.

Montone, P. and Mariucci, M. T.: The new release of the Italian contemporary stress map, Geophys. J. Int., 205, 1525–1531, https://doi.org/10.1093/gji/ggw100, 2016.

Montone, P. and Mariucci, M. T.: Constraints on the Structure of the Shallow Crust in Central Italy from Geophysical Log Data, Sci. Rep.-UK, 10, 3834, https://doi.org/10.1038/s41598-020-60855-0, 2020.

Montone, P. and Mariucci, M. T.: Lateral Variations of P-Wave Velocity from Deep Borehole Data in the Southern Apennines, Italy, Pure Appl. Geophys., 180, 1925–1944, https://doi.org/10.1007/s00024-023-03248-4, 2023.

Pierdominici, S. and Kück, J.: Borehole Geophysics, in: Encyclopedia of Geology, 2nd edn., Elsevier, 746–760, https://doi.org/10.1016/B978-0-08-102908-4.00126-0, 2021.

Pierdominici, S., Millett, J. M., Kück, J. K. M., Thomas, D., Jerram, D. A., Planke, S., Haskins, E., Lautze, N., and Galland, O.: Stress field interactions between overlapping shield volcanoes: Borehole breakout evidence from the island of Hawaii, USA, J. Geophys. Res., 125, e2020JB019768, https://doi.org/10.1029/2020JB019768, 2020.

Pizzi, A., Di Domenica, A., Gallovic, F., Luzi, L., and Puglia, R.: Fault segmentation as constraint to the occurrence of the main shocks of the 2016 Central Italy seismic sequence, Tectonics, 36, 2370–2387, https://doi.org/10.1002/2017TC004652, 2017.

Pondrelli, S. and Salimbeni, S.: Italian CMT Dataset [data set], Istituto Nazionale di Geofisica e Vulcanologia (INGV), https://doi.org/10.13127/rcmt/italy, 2006.

Pondrelli, S., Salimbeni, S., Ekström, G., Morelli, A., Gasperini, P., and Vannucci, G.: The Italian CMT dataset from 1977 to the present, Phys. Earth Planet. In., 159, 286–303, https://doi.org/10.1016/j.pepi.2006.07.008, 2006.

Porreca, M., Minelli, G., Ercoli, M., Brobia, A., Mancinelli, P., Cruciani, F., Giorgetti, C., Carboni, F., Mirabella, F., Cavinato, G., Cannata, A., Pauselli, C., and Barchi, M. R.: Seismic reflection profiles and subsurface geology of the area interested by the 2016–2017 earthquake sequence (Central Italy), Tectonics, 37, 1116–1137, https://doi.org/10.1002/2017TC004915, 2018.

Price, N. J.: Fault and Joint Development in Brittle and Semi-Brittle Rocks, Pergamon Press, Oxford, ISBN 1483169782, 1966.

Rider, M. H. and Kennedy, M.: The Geological Interpretation of Well Logs, Rider-French, Scotland, 432 pp., ISBN 10:0954190688, 2011.

Schön, J. H.: Physical Properties of Rocks – Fundamentals and Principles of Petrophysics, in: 2nd Edn., Elsevier, ISBN 9780081004043, 2015.

Scisciani, V., Agostini, S., Calamita, F., Pace, P., Cilli, A., Giori, I., and Paltrinieri, W.: Positive inversion tectonics in foreland fold-and thrust belts: a reappraisal of the Umbria–Marche northern Apennines (Central Italy) by integrating geological and geophysical data, Tectonophysics, 637, 218–237, https://doi.org/10.1016/j.tecto.2014.10.010, 2014.

Serra, O.: Fundamentals of well-log interpretation. Part 1: The acquisition of logging data, Developments in petroleum science 15A, Elsevier, Amsterdam, 435 pp., ISBN 0-444-42132-7, 1984.

Smeraglia, L., Trippetta, F., Carminati, E., and Mollo, S.: Tectonic control on the petrophysical properties of foredeep sandstone in the Central Apennines, Italy, J. Geophys. Res., 119, 9077–9094, 2014.

Terzaghi, R. D.: Sources of error in joint surveys, Geotechnique, 15, 287–304, https://doi.org/10.1680/geot.1965.15.3.287, 1965.

Tinti, E., Scognamiglio, L., Michelini, A., and Cocco, M.: Slip heterogeneity and directivity of the M_L 6.0 2016 Amatrice earthquake estimated with rapid finite-fault inversion, Geophys. Res. Lett., 43, 10745–10752, https://doi.org/10.1002/2016GL071263, 2016.

Trippetta, F., Collettini, C., Vinciguerra, S., and Meredith, P. G.: Laboratory measurements of the physical properties of Triassic evaporites from central Italy and correlation with geophysical data, Tectonophysics, 492, 121–132, https://doi.org/10.1016/j.tecto.2010.06.001, 2010.

Trippetta, F., Barchi, M. R., Tinti, E., Volpe, G., Rosset, G., and De Paola, N.: Lithological and stress anisotropy control large-scale seismic velocity variations in tight carbonates, Sci. Rep.-UK, 11, 9472, https://doi.org/10.1038/s41598-021-89019-4, 2021.

Valoroso, L., Chiaraluce, L., Piccinini, D., Di Stefano, R., and Waldhauser, F.: Radiography of a normal fault system by 64 000 high-precision earthquake locations: The 2009 L'Aquila (central Italy) case study, J. Geophys. Res.-Sol. Ea., 118, 1156–1176, https://doi.org/10.1002/jgrb.50130, 2013.

Valoroso, L., Chiaraluce, L., Di Stefano, R., and Monachesi, G.: Mixed-mode slip behaviour of the Altotiberina low-angle normal fault system (Northern Apennines, Italy) through high-resolution earthquake locations and repeating events, J. Geophys. Res.-Sol. Ea., 122, 10220–10240, https://doi.org/10.1002/2017JB014607, 2017.

Villani, F., Civico, R., Pucci, S., Pizzimenti, L., Nappi, R., De Martini, P. M., and the Open EMERGEO Working Group: A database of the coseismic effects following the 30 October 2016 Norcia earthquake in Central Italy, Scientific Data, 5, 180049, https://doi.org/10.1038/sdata.2018.49, 2018.

Vuan, A., Brondi, P., Sugan, M., Chiaraluce, L., Di Stefano, R., and Michele, M.: Intermittent slip along the Alto Tiberina low angle normal fault in central Italy, Geophys. Res. Lett., 47, e2020GL08903, https://doi.org/10.1029/2020GL089039, 2020.